**Atmospheric
Chemistry
and Physics**

Mass-based hygroscopicity parameter interaction model and measurement of atmospheric aerosol water uptake

E. Mikhailov[1,2], S. Vlasenko[2], D. Rose[1], and U. Pöschl[1]

[1]Multiphase Chemistry and Biogeochemisty Departments, Max Planck Institute for Chemistry, Mainz, Germany
[2]Atmospheric Physics Department, Institute of Physics, St. Petersburg State University, St. Petersburg, Russia

Correspondence to: E. Mikhailov (eugene.mikhailov@paloma.spbu.ru)

Abstract. In this study we derive and apply a mass-based hygroscopicity parameter interaction model for efficient description of concentration-dependent water uptake by atmospheric aerosol particles with complex chemical composition. The model approach builds on the single hygroscopicity parameter model of Petters and Kreidenweis (2007). We introduce an observable mass-based hygroscopicity parameter κ_m which can be deconvoluted into a dilute hygroscopicity parameter (κ_m^0) and additional self- and cross-interaction parameters describing non-ideal solution behavior and concentration dependencies of single- and multi-component systems.

For reference aerosol samples of sodium chloride and ammonium sulfate, the κ_m-interaction model (KIM) captures the experimentally observed concentration and humidity dependence of the hygroscopicity parameter and is in good agreement with an accurate reference model based on the Pitzer ion-interaction approach (Aerosol Inorganic Model, AIM). Experimental results for pure organic particles (malonic acid, levoglucosan) and for mixed organic-inorganic particles (malonic acid – ammonium sulfate) are also well reproduced by KIM, taking into account apparent or equilibrium solubilities for stepwise or gradual deliquescence and efflorescence transitions.

The mixed organic-inorganic particles as well as atmospheric aerosol samples exhibit three distinctly different regimes of hygroscopicity: (I) a quasi-eutonic deliquescence & efflorescence regime at low-humidity where substances are just partly dissolved and exist also in a non-dissolved phase, (II) a gradual deliquescence & efflorescence regime at intermediate humidity where different solutes undergo gradual dissolution or solidification in the aqueous phase; and (III) a dilute regime at high humidity where the solutes are fully dissolved approaching their dilute hygroscopicity.

For atmospheric aerosol samples collected from boreal rural air and from pristine tropical rainforest air (secondary organic aerosol) we present first mass-based measurements of water uptake over a wide range of relative humidity (1–99.4 %) obtained with a new filter-based differential hygroscopicity analyzer (FDHA) technique. For these samples the concentration dependence of κ_m can be described by a simple KIM model equation based on observable mass growth factors and a total of only six fit parameters summarizing the combined effects of the dilute hygroscopicity parameters, self- and cross-interaction parameters, and solubilities of all involved chemical components. One of the fit parameters represents κ_m^0 and can be used to predict critical dry diameters for the activation of cloud condensation nuclei (CCN) as a function of water vapor supersaturation according to Köhler theory. For sodium chloride and ammonium sulfate reference particles as well as for pristine rainforest aerosols consisting mostly of secondary organic matter, we obtained good agreement between the KIM predictions and measurement data of CCN activation.

The application of KIM and mass-based measurement techniques shall help to bridge gaps in the current understanding of water uptake by atmospheric aerosols: (1) the gap between hygroscopicity parameters determined by hygroscopic growth measurements under sub-saturated conditions and by CCN activation measurements at water vapor supersaturation, and (2) the gap between the results of simplified single parameter models widely used in atmospheric or climate science and the results of complex multi-parameter ion- and molecule-interaction models frequently used in physical chemistry and solution thermodynamics (e.g., AIM, E-AIM, ADDEM, UNIFAC, AIOMFAC).

1 Introduction

The interaction of aerosol particles with water vapor is among the central issues of current research in atmospheric and climate science, and numerous studies have investigated the hygroscopicity of aerosol particles and their ability to serve as cloud condensation nuclei (CCN). Köhler theory is the main tool to describe the hygroscopic growth of particles as a function of relative humidity (e.g., Pruppacher and Klett, 2000; Seinfeld and Pandis, 2006), and various types of Köhler models have been developed and applied for the analysis of laboratory and field measurement results as well as in numerical models of the atmosphere and climate (e.g., Junge and McLaren, 1971; Fitzgerald, 1973, Shulman et al., 1996; Kulmala et al., 1997; Laaksonen et al., 1998, Raymond and Pandis, 2003; Bilde and Svenningsson, 2004; Mikhailov et al., 2004, 2009; Huff Hartz et al., 2005; McFiggans et al., 2006; Svenningsson et al., 2006; Rose et al., 2008; and references therein).

A central aim of hygroscopicity measurements and Köhler model studies is to relate the critical supersaturation of CCN activation to the hygroscopic growth factors observed at subsaturated conditions (e.g., Rissler et al., 2004; Kreidenweis et al., 2005; Mochida et al., 2006; Petters and Kreidenweis, 2007; Wex et al., 2008; Gunthe et al., 2009; Petters et al., 2009; Good et al., 2010a, b; Irwin et al., 2010; Roberts et al., 2010; Cerully et al., 2011; Duplissy et al., 2011; Fors et al., 2011; Metzger et al., 2012; and references therein). For this purpose, Petters and Kreidenweis (2007) proposed a single-parameter Köhler model where the hygroscopicity parameter κ provides a volume-based measure of aerosol water uptake characteristics and CCN activity. For water soluble organic and inorganic compounds, the relative differences between κ values derived from CCN and growth factor measurements are usually less than 30 % and can be explained by non-ideal behavior of concentrated solutions (e.g., Wex et al., 2008; Mikhailov et al., 2009). For particles containing sparingly soluble compounds, however, the differences can increase by a factor of 5 or more (Petters and Kreidenweis, 2007). To bridge the gap between κ values observed under subsaturated and supersaturated conditions, Petters and Kreidenweis (2008) proposed a pseudo-two-component κ-Köhler model where sparingly soluble compounds gradually enter the solution with increasing dilution and relative humidity. The practical applicability of volume based hygroscopicity models, however, is often limited by deviations from volume-additivity and by the effects of capillary condensation and restructuring of porous and irregularly shaped particles (e.g., Krämer et al., 2000; Mikhailov et al., 2004, 2009; Gysel et al., 2004; Sjogren et al., 2007; Zardini et al., 2008; Wang et al., 2010).

Detailed thermodynamic models that describe the water uptake of aqueous solutions and aerosols are usually mass-based rather than volume-based and require multiple input parameters for every chemical species involved. For example, seven parameters are used to describe a simple NaCl particle with the rigorous Aerosol Inorganic Model (AIM; Clegg et al., 1998; Wexler and Clegg, 2002; http://www.aim.env.uea.ac.uk/aim/aim.php). Other advanced models like the Extended Aerosol Inorganic Model (E-AIM; Clegg et al., 2001), the Aerosol Diameter Dependent Equilibrium Model (AD-DEM, Topping et al., 2005a, b), the Universal Quasichemical Functional Group Activity Coefficients model (UNIFAC; Fredenslund et al., 1975; Hansen et al., 1991), the Aerosol Inorganic-Organic Mixtures Functional Groups Activity Coefficients model (AIOMFAC; Zuend et al., 2008, 2011) and related approaches referenced in the above studies typically also require four or more semi-empirical parameters for single solute systems plus additional interaction parameters for multi-component systems. Application of these complex thermodynamic models to atmospheric aerosols containing a multitude of unspeciated organic compounds remains difficult, especially at low relative humidity (RH) (Petters and Kreidenweis, 2007; Tong et al., 2008).

In this study we introduce a mass-based hygroscopicity parameter κ_m building on the single hygroscopicity parameter of Petters and Kreidenweis (2007), and we develop a κ_m-interaction model (KIM), which describes the non-ideal solution behavior and concentration dependence of single- and multi-component systems with a small number of parameters that can be determined by fitting of measurement data. We demonstrate that the KIM approach can capture and reproduce the characteristics of water uptake by reference substances as well as atmospheric aerosol samples under sub- and supersaturated conditions.

2 Theory

2.1 Volume-based hygroscopicity parameter κ_v

The Köhler theory relates the water activity (a_w), the partial molar volume of water ($\overline{V}_w$), the surface tension (σ), and the diameter (D) of a spherical aqueous droplet under equilibrium conditions to the water vapor saturation of the surrounding gas phase ($s_w = \text{RH}/100\%$) (e.g., Pruppacher and Klett, 2000; Seinfeld and Pandis, 2006):

$$s_w = a_w \exp\left(\frac{4\sigma \overline{V}_w}{RTD}\right), \tag{1}$$

where R is the universal gas constant and T is the temperature. Note that all frequently used symbols used in this manuscript are also explained in Table 1.

According to Petters and Kreidenweis (2007), the hygroscopic growth of aerosol particles can be efficiently approximated by a simplified version of Eq. (1), the so-called κ_v-Köhler equation:

Table 1. Frequently used symbols.

Symbol	SI Unit	Quantity
a_w		water activity
C_m	kg kg^{-1}	solubility (gram solute per gram water)
C_m^{eu}	kg kg^{-1}	eutonic solubility (gram solute per gram water)
$C_{m,i}^{ap}$	kg kg^{-1}	apparent solubility (gram solute per gram water)
$c_{m,i}$	kg kg^{-1}	mass concentration (gram solute per gram water)
D	m	diameter of aqueous solution droplet
D_d	m	diameter of dry aerosol particle
$D_{d,c}$	m	critical dry diameter of CCN activation
f_i		mass fraction of individual component in particulate matter
G_D		diameter growth factor
G_m		mass growth factor
J		van't Hoff factor
m_d	kg	mass of the dry solute in aqueous droplet
M_w	kg mol^{-1}	molar mass of pure water
m_w	kg	mass of the water in aqueous droplet
R	J K^{-1} mol^{-1}	universal gas constant
s_w		water vapor saturation ratio
S_w	%	water vapor supersaturation
$s_{w,c}$		critical water vapor saturation ratio
T	K	temperature
α_{ij}, α_{ii}		cross- and self-interaction coefficients
κ_v		volume-based hygroscopicity parameter
κ_m		mass-based hygroscopicity parameter
κ_m^0		mass-based dilute hygroscopicity
μ	mol kg^{-1}	molality (mole solute per kilogram water)
ρ_d	kg m^{-3}	density of dry particle material
ρ_w	kg m^{-3}	density of pure water
σ	J m^{-2}	surface tension of solution droplet
σ_w	J m^{-2}	surface tension of pure water
RH$_d$	%	deliquescence relative humidity of individual component
RH$_e$	%	efflorescence relative humidity of individual component

$$s_w \approx a_w \exp\left(\frac{4\sigma_w M_w}{RT\rho_w D}\right)$$

$$= \left[\frac{\kappa_v}{G_D^3 - 1} + 1\right]^{-1} \exp\left(\frac{4\sigma_w M_w}{RT\rho_w G_D D_d}\right) \quad (2)$$

Here M_w, σ_w and ρ_w are the molar mass, surface tension, and density of pure water. The diameter growth factor G_D is defined as the ratio between the volume equivalent diameters of the aqueous droplet and of the dry aerosol particle ($G_D = D/D_d$).

The hygroscopicity parameter κ_v relates the volume of the dry aerosol particle (V_d) to the volume of water (V_w) and the activity of water (a_w) in the aqueous droplet:

$$\frac{1}{a_w} = 1 + \kappa_v \frac{V_d}{V_w} \quad (3)$$

$$a_w = \left(\frac{\kappa_v}{G_D^3 - 1} + 1\right)^{-1} \quad (4)$$

Equations (2)–(4) are commonly used to determine effective hygroscopicity parameters from hygroscopic growth or CCN activation measurements using hygroscopicity tandem differential mobility analyzer (HTDMA) and CCN counter techniques (e.g.: Petters and Kreidenweis, 2007; Petters et al., 2009; Gunthe et al., 2009; Mikhailov et al., 2009; Carrico et al., 2010; Rose et al., 2010, 2011; Duplissy et al., 2011 and references therein). In the analysis of laboratory and field measurement data it is often assumed that measured mobility equivalent diameters (D, D_d) can be regarded as volume equivalent diameters, and that the volume change of mixing is negligible ("volume additivity assumption"). The limitations of these assumptions for HTDMA and CCN experiments have been outlined and discussed in earlier studies (e.g., Krämer et al., 2000; Gysel et al., 2002; Rose et al., 2008; Mikhailov et al., 2004, 2009; Wang et al., 2010; and references therein). For an individual solute (i), the

hygroscopicity parameter can be related to the molar mass (M_i), density (ρ_i), and the van't Hoff factor or effective dissociation number (J_i) of the solute:

$$\kappa_{v,i} = J_i \frac{\rho_i / M_i}{\rho_w / M_w} \tag{5}$$

Thus, $\kappa_{v,i}$ can be regarded as an effective molar density of ions or molecules in the solute normalized by the molar density of water ($\rho_w / M_w \approx 55\,\mathrm{mol\,L^{-1}}$) which has been designated as "effective Raoult parameter" or "dilute hygroscopicity" of the solute (Mikhailov et al., 2009; Sullivan et al., 2009).

In concentrated solutions, $\kappa_{v,i}$ is usually concentration-dependent (Mikhailov et al., 2009), but under dilute conditions it approaches a substance-specific fixed value which we designate as the "dilute hygroscopicity", $\kappa_{v,i}^0$. This parameter is easy to calculate from tabulated values of J_i for dilute aqueous solutions (Eq. 5).

2.2 Mass-based hygroscopicity parameter κ_m

In analogy to the volume-based hygroscopicity parameter (Eq. 3), we define a mass-based hygroscopicity parameter κ_m:

$$\frac{1}{a_w} = 1 + \kappa_m \frac{m_d}{m_w}, \tag{6}$$

where m_d is the mass of the dry particle material and m_w is the mass of water in the wet particle (aqueous droplet).

Under the assumption of volume additivity, Eq. (3) and Eq. (6) can be combined to

$$\kappa_m = \kappa_v \frac{\rho_w}{\rho_d} \tag{7}$$

where ρ_d is the density of the dry particle material. In this case, the knowledge of ρ_d enables conversion of κ_v into κ_m and vice versa. On the other hand, independent measurements of κ_v and κ_m enable the determination of ρ_d.

The mass-based dilute hygroscopicity, $\kappa_{m,i}^0$, follows from Eq. (5) and Eq. (7); it is the van't Hoff factor for a dilute solution (J_i^0) scaled by the ratio of the molar masses of water and solute:

$$\kappa_{m,i}^0 = J_i^0 \frac{M_w}{M_i} \tag{8}$$

By defining the mass growth factor G_m as

$$G_m = \frac{m_w + m_d}{m_d} \tag{9}$$

and combining Eq. (9) and Eq. (6) we obtain

$$a_w = \left(\frac{\kappa_m}{G_m - 1} + 1 \right)^{-1} \tag{10}$$

The mass-based relation between water activity and particle hygroscopicity specified in Eq. (10) is equivalent to the volume based formulation in Eq. (4). Due to mass conservation,

however, the practical applicability of Eq. (10) and the precision of related parameters determined in mass-based experiments is not affected by deviations from spherical geometry and volume additivity that usually limit the applicability and precision of volume-based parameters determined in mobility diameter-based HTDMA and CCN experiments (e.g., Krämer et al., 2000; Gysel et al., 2002, 2004; Rose et al., 2008; Mikhailov et al., 2004, 2009; Wang et al., 2010; and references therein).

The mass-based definition of the hygroscopicity parameter κ_m (Eq. 6) avoids a complication that occurs in the volume-based definition of κ_v (Eq. 3): the theoretical distinction and practical determination of specific volume vs. partial specific volume (alias molar vs. partial molar volume) of water and solute in a solution droplet. This distinction had not been addressed and specified in the original volume-based definition of κ_v (Petters and Kreidenweis, 2007), but it is relevant in systems where the volumes of mixed components are not linearly additive.

If the densities of the dry solute and of the solution are known, the masses of dry particles and aqueous droplets can be easily converted into volume equivalent diameters: $D_d^3 = 6m_d / (\pi \rho_d)$, $D^3 = 6G_m m_d / (\pi \rho)$, and $D = D_d \left(G_m \rho_d / \rho \right)^{1/3}$, where ρ is the density of the aqueous solution droplet. For dilute aqueous solution droplets with $\rho \approx \rho_w$ follows

$$D = D_d \left(G_m \frac{\rho_d}{\rho_w} \right)^{1/3} \tag{11}$$

By inserting Eq. (10) and Eq. (11) in Eq. (2), we obtain an approximate mass-based κ_m-Köhler equation:

$$\frac{\mathrm{RH}}{100\,\%} = s_w \approx \left(\frac{\kappa_m}{G_m - 1} + 1 \right)^{-1} \exp\left(\frac{4\sigma_w M_w}{RT\rho_w D_d} \left[\frac{\rho_w}{\rho_d G_m} \right]^{1/3} \right) \tag{12}$$

The critical mass growth factor ($G_{m,c}$) and the critical water vapor saturation ratio ($s_{w,c}$) for the CCN activation of an aerosol particle with dry diameter D_d and hygroscopicity κ_m correspond to the maximum value of s_w according to Eq. (12) ($ds_w/dG_m = 0$):

$$G_{m,c} = \left(\frac{3\kappa_m D_d}{A} \right)^{3/2} \left(\frac{\rho_d}{\rho_w} \right)^{1/2} \tag{13}$$

$$s_{w,c} = \exp\left[\frac{2}{3} \left(\frac{A}{D_d} \right)^{3/2} \left(\frac{\rho_w}{3\kappa_m \rho_d} \right)^{1/2} \right] \tag{14}$$

with $A = \frac{4\sigma_w M_w}{RT\rho_w}$.

Exponential series expansion, cancellation of higher order terms, and rearrangement of Eq. (14) lead to the following approximate relation between the critical dry diameter of CCN activation ($D_{d,c}$) and water vapor supersaturation ($S_w = (s_w - 1) \cdot 100\,\%$):

$$D_{d,c} = A \cdot \left(\frac{4\rho_w}{27\kappa_m \rho_d} \right)^{1/3} \left(\frac{S_w}{100\,\%} \right)^{-2/3} = \beta \cdot S_w^{-2/3} \tag{15}$$

with $\beta = A \cdot \left(\frac{4\rho_w}{27\kappa_m\rho_d}\right)^{1/3}\left(\frac{1}{100\%}\right)^{-2/3}$. A detailed derivation of Eq. (15) is given in Appendix A.

2.3 Hygroscopicity parameter interaction model (KIM)

In analogy to Petters and Kreidenweis (2008, Eq. 10), the mass-based hygroscopicity parameter of a multi-component particle can be approximated by a simple mixing rule that builds on the Zdanovskii-Stokes-Robinson (ZSR) approach (Stokes and Robinson, 1966; Seinfeld and Pandis, 2006):

$$\kappa_m = \sum_i f_i \kappa_{m,i} H\left(y_{m,i}\right)$$
$$y_{m,i} = (G_m - 1)C_{m,i}/f_i \qquad (16)$$
$$H\left(y_{m,i}\right) = \begin{cases} y_{m,i} & \text{if } y_{m,i} < 1 \quad \text{(partly dissolved)} \\ 1 & \text{if } y_{m,i} \geq 1 \quad \text{(fully dissolved)} \end{cases}$$

Here f_i is the dry mass fraction of the solute component i, $C_{m,i}$ is the solubility of the solute in water (mass of dissolved compound i per unit mass of water under equilibrium conditions), and $H(y_{m,i})$ is the relative fraction of component i that is actually dissolved in the aqueous phase. Accordingly, water insoluble components with $\kappa_m \approx 0$ do not contribute to the overall particle hygroscopicity. For completely dissolved particles, all values of $y_{m,i}$ equal unity, and κ_m is given by the simple relation

$$\kappa_m = \sum_i f_i \kappa_{m,i} \qquad (17)$$

Note that in Eq. (16) and Eq. (17) the hygroscopicity parameters of individual chemical components $\kappa_{m,i}$ are weighted by the corresponding mass fractions, f_i, which are usually easier to determine than the volume fractions. Due to the difficulties involved in obtaining correct density estimates for mixtures of organic and inorganic compounds in atmospheric aerosol particles, many recent studies applying a hygroscopicity parameter mixing rule used mass fractions as a proxy for volume fractions (e.g., Kreidenweis et al., 2008; Gunthe et al., 2009, 2011; Pringle et al., 2010; Rose et al., 2011).

In the highly dilute solution droplets usually formed at high RH and upon CCN activation, the hygroscopicity parameters of individual solute components ($\kappa_{m,i}$) approach the dilute hygroscopicity values $\kappa_{m,i}^0$ that can be estimated using Eq. (8) and inserted in Eq. (16) or Eq. (17), respectively.

In the highly concentrated solutions formed at low RH, however, the hygroscopicity of aerosol particles does not always follow the simple ZSR approach (ideal mixing). Interactions between solute ions and molecules can lead to either higher or lower solubilities and hygroscopicity parameters as compared to single-component and dilute solutions (Marcolli et al., 2004; Marcolli and Krieger, 2006; Mikhailov et al., 2009).

To describe the non-ideal behavior of concentrated solutions, we propose a hygroscopicity parameter interaction model, briefly κ_m-interaction model (KIM), that combines dilute hygroscopicity parameters with additional terms

of cross- or self-interaction between molecular and ionic species:

$$\kappa_m = \sum_i K_{m,i}, \qquad (18)$$

where the parameter $K_{m,i}$ for each component is defined by

$$K_{m,i} = \begin{cases} \left(\kappa_{m,i}^0 + \delta\kappa_{m,ij} + \delta\kappa_{m,ii}\right)(G_m - 1)C_{m,i} \\ \quad \text{if } (G_m - 1)C_{m,i} < f_i \quad \text{(partly dissolved)} \\ \left(\kappa_{m,i}^0 + \delta\kappa_{m,ij} + \delta\kappa_{m,ii}\right)f_i \\ \quad \text{if } (G_m - 1)C_{m,i} \geq f_i \quad \text{(fully dissolved)} \end{cases} \qquad (19)$$

Here $\delta\kappa_{m,ij}$ and $\delta\kappa_{m,ii}$ are defined as incremental hygroscopicity terms accounting for cross- and self-interactions of molecular and ionic species, respectively. Accounting of binary interactions between solutes in the aqueous solution droplet (Clegg et al., 2001, 2003), the concentration dependence of the incremental terms $\delta\kappa_{m,ij}$ and $\delta\kappa_{m,ii}$ can be described by:

$$\delta\kappa_{m,ij} = c_{m,i}\sum_{i>j}\alpha_{ij}c_{m,j}$$
$$\delta\kappa_{m,ii} = \alpha_{ii}c_{m,i}^2 \qquad (20)$$

Here α_{ij} and α_{ii} are cross- and self-interaction coefficients, respectively; $c_{m,i}$ and $c_{m,j}$ are the mass concentrations of individual components (i, j) in the aqueous solution expressed here as mass of solute per unit mass of water. Depending on the nature of solute interaction, the interaction coefficients and the resulting incremental hygroscopicity terms can assume positive or negative values. Accordingly, the concentration dependence of κ_m can be expressed as follows:

$$\kappa_m = \sum_i \kappa_{m,i}^0 c_{m,i} + \sum_i \sum_{j>i}\alpha_{ij}c_{m,i}c_{m,j} + \sum_i \alpha_{ii}c_{m,i}^2 \qquad (21)$$

In the double sum on the right hand side of Eq. (21), self-interactions are excluded and each pair of solutes is counted only once $(j > i)$. The mass concentration of each component in the aqueous solution, $c_{m,i}$, can be calculated either from the solubility $C_{m,i}$ (if component i is only partially dissolved) or from the dry mass fraction f_i (if component i is fully dissolved):

$$c_{m,i} = \begin{cases} C_{m,i} & \text{if } (G_m - 1)C_{m,i} < f_i \\ f_i/(G_m - 1) & \text{if } (G_m - 1)C_{m,i} \geq f_i \end{cases} \qquad (22)$$

For a system consisting of fully dissolved (fd) and partly dissolved (pd) components, Eq. (18) to Eq. (22) can be combined into:

$\kappa_{\mathrm{m}} =$

$$\sum_{i \in \mathrm{pd}} \left(\kappa^0_{\mathrm{m},i} + C_{\mathrm{m},i} \left[\sum_{j \in \mathrm{fd}} \alpha_{ij} \frac{f_j}{G_{\mathrm{m}}-1} + \sum_{\substack{j \in \mathrm{pd}, \\ j > i}} \alpha_{ij} C_{\mathrm{m},j} \right] + \alpha_{ii} C^2_{\mathrm{m},i} \right)$$
$$(G_{\mathrm{m}}-1) C_{\mathrm{m},i} + \tag{23}$$

$$\sum_{i \in \mathrm{fd}} \left(\kappa^0_{\mathrm{m},i} + \frac{f_i}{(G_{\mathrm{m}}-1)} \left[\sum_{\substack{j \in \mathrm{fd}, \\ j > i}} \alpha_{ij} \frac{f_j}{G_{\mathrm{m}}-1} + \sum_{j \in \mathrm{pd}} \alpha_{ij} C_{\mathrm{m},j} \right] + \alpha_{ii} \frac{f_i^2}{(G_{\mathrm{m}}-1)^2} \right) f_i$$

where

$$\begin{aligned} i \in \mathrm{pd}, &\text{ if } (G_{\mathrm{m}}-1) C_{\mathrm{m},i} < f_i \\ i \in \mathrm{fd}, &\text{ if } (G_{\mathrm{m}}-1) C_{\mathrm{m},i} \geq f_i \end{aligned}. \tag{24}$$

Here the designation $i \in \mathrm{pd}$ means that component i is only partially dissolved in the aqueous phase, while the designation $i \in \mathrm{fd}$ refers to a component that is fully dissolved in the aqueous phase. For $i \in \mathrm{pd}$ the aqueous phase concentration $c_{\mathrm{m},i}$ depends on $C_{\mathrm{m},i}$, and for $i \in \mathrm{fd}$ the aqueous phase concentration $c_{\mathrm{m},i}$ depends on G_{m} and f_i as specified in Eq. (22).

In multi-component systems, the solubility of an individual component $C_{\mathrm{m},i}$ in the mixture is not necessarily the same as the solubility of the component in pure water, $C_{\mathrm{m,w},i}$ (single-component system). Interactions between different substances can increase or decrease the solubility of individual components (Marcolli et al., 2004; Marcolli and Krieger, 2006). The influence of multiple solutes on the solubility of individual components can be described according to the Setschenov equation (Setschenov, 1889):

$$C_{\mathrm{m},i}/C_{\mathrm{m,w},i} = \exp \left[\sum_{j \in \mathrm{pd}} \eta_{ij} C_{\mathrm{m},j} + \sum_{j \in \mathrm{fd}} \eta_{ij} \left(\frac{f_j}{G_{\mathrm{m}}-1} \right) \right], \tag{25}$$

where η_{ij} is the salting out constant.

If all substances are just partly dissolved (pd) and exist also in a non-dissolved phase, the concentration of each component is given by the eutonic solubility, $C^{\mathrm{eu}}_{\mathrm{m},i}$. In this case, Eq. (23) can be reduced to

$$\kappa_{\mathrm{m}} = \sum_{i \in \mathrm{pd}} \left(\kappa^0_{\mathrm{m},i} + C^{\mathrm{eu}}_{\mathrm{m},i} \sum_{\substack{j \in \mathrm{pd}, \\ j > i}} \alpha_{ij} C^{\mathrm{eu}}_{\mathrm{m},j} + \alpha_{ii} (C^{\mathrm{eu}}_{\mathrm{m},i})^2 \right)$$
$$(G_{\mathrm{m}}-1) C^{\mathrm{eu}}_{\mathrm{m},i}. \tag{26}$$

Combining Eq. (26) with Eq. (10) yields a constant water activity independent of G_{m}, which is characteristic for stepwise phase transitions (deliquescence or efflorescence). The term eutonic solubility normally refers to a liquid phase in stable equilibrium with multiple crystalline phases. Partly dissolved solutes may also co-exist in meta-stable equilibrium with amorphous phases. For this "quasi-eutonic" state, the maximum aqueous phase concentration of a solute can be

characterized by an apparent solubility, $C^{\mathrm{ap}}_{\mathrm{m},i}$ replacing the eutonic solubility $C^{\mathrm{eu}}_{\mathrm{m},i}$ in Eq. (26). Apparent solubilities are well-established parameters for the description of the water interactions of amorphous substances as discussed below and in the scientific literature dealing with semi-solid or solid amorphous organics in the pharmaceutical and food sciences (Mosharraf and Nyström, 1999; Hancock and Parks, 2000; Murdande et al., 2010, 2011). In contrast to the thermodynamically fixed value of equilibrium solubility, however, the apparent solubility of a substance is a kinetically limited parameter that may vary depending on the pre-treatment and history of the investigated system. The apparent solubility enhancement ratio $R_{\mathrm{ap},i} = C^{\mathrm{ap}}_{\mathrm{m},i} / C_{\mathrm{m},i}$ can be used to describe the degree of supersaturation and amorphicity/metastability of the system (Hancock and Parks, 2000; Murdande et al., 2010, 2011).

If all substances are completely dissolved, Eq. (23) can be reduced to

$$\kappa_{\mathrm{m}} = \sum_{i \in \mathrm{fd}} \left(\kappa^0_{\mathrm{m},i} + \frac{f_i}{(G_{\mathrm{m}}-1)} \sum_{\substack{j \in \mathrm{fd}, \\ j > i}} \alpha_{ij} \frac{f_j}{(G_{\mathrm{m}}-1)} + \alpha_{ii} \frac{f_i^2}{(G_{\mathrm{m}}-1)^2} \right) f_i \tag{27}$$

In case of dilute solutions ($G_{\mathrm{m}} \gg 1$), the relative importance of the incremental hygroscopicity terms decreases and Eq. (27) can be further reduced to Eq. (17).

For a single component system with $f_i = 1$, $f_j = 0$, and $\alpha_{ii} = \alpha$, Eq. (23) can be simplified to

$$\kappa_{\mathrm{m}} = \left(\kappa^0_{\mathrm{m}} + \alpha C^2_{\mathrm{m}} \right) (G_{\mathrm{m}}-1) C_{\mathrm{m}} \tag{28}$$
if $(G_{\mathrm{m}}-1) C_{\mathrm{m}} < 1$ (partly dissolved)

$$\kappa_{\mathrm{m}} = \kappa^0_{\mathrm{m}} + \frac{\alpha}{(G_{\mathrm{m}}-1)^2} \tag{29}$$
if $(G_{\mathrm{m}}-1) C_{\mathrm{m}} \geq 1$ (fully dissolved)

Equation (29) can be combined with Eq. (8), Eq. (10), and with the relation

$$c_{\mathrm{m}} = (G_{\mathrm{m}}-1)^{-1} = \mu M \tag{30}$$

to obtain an explicit expression of water activity in the aqueous solution of a fully dissolved single solute with molar mass M, molality μ and van't Hoff factor J^0:

$$a_{\mathrm{w}} = \left(1 + \kappa^0_{\mathrm{m}} c_{\mathrm{m}} + \alpha c^3_{\mathrm{m}} \right)^{-1} = \left(1 + \frac{\kappa^0_{\mathrm{m}}}{(G_{\mathrm{m}}-1)} + \frac{\alpha}{(G_{\mathrm{m}}-1)^3} \right)^{-1}$$
$$= \left(1 + J^0 \mu M_{\mathrm{w}} + \alpha (\mu M)^3 \right)^{-1} \tag{31}$$

This expression represents a middle way between the simplistic assumption of a constant single hygroscopicity parameter and the complex multi-parameter models typically using four or more semi-empirical parameters for a single solute system (e.g.: AIM, E-AIM, ADDEM, UNIFAC, AIOMFAC as specified in the introduction). Note that the

Table 2. Atmospheric aerosol samples.

Sample	Sampling location	Sampling height above ground (m)	Sampling period	Aerosol mass used for FDHA analysis (mg)
AMAZE	Manaus, Brazil 02°35′ S, 60°12′ W	39	15–20 Feb 2008	0.061 ±0.002
SPB	Saint-Petersburg, Russia 59°88′ N, 29°82′ E	15	18–27 May 2009	0.60 ±0.01

more detailed solute interaction models are generally also mass-based rather than volume-based for the reasons outlined above (mass conservation vs. volume non-additivity).

Inserting the equilibrium solubility C_m for the mass concentration c_m in Eq. (31) and combination with Eq. (12) leads to the following explicit analytical expression for the relative humidity threshold of the deliquescence of solid particles (RH$_d$):

$$\mathrm{RH}_d \approx 100 \times \left[\left(\kappa_m^0 + \alpha C_m^2 \right) + 1 \right]^{-1}$$
$$\exp \left[\frac{4\sigma_w M_w}{RT\rho_w D_d} \left(\frac{\rho_w}{\rho_d \left(C_m^{-1} + 1 \right)} \right)^{1/3} \right] \tag{32}$$

The same equation yields the relative humidity threshold of the efflorescence of supersaturated solution droplets (RH$_e$) when the apparent solubility $C_{m,i}^{ap}$ as defined and used below is inserted (Sect. 4.1).

General relations between the KIM approach, the osmotic coefficient of multi-component aqueous solutions, and the extended ZSR model approach of Clegg et al. (2003) are specified and discussed in Appendix B.

3 Experiments

3.1 Aerosol sampling and composition

Atmospheric aerosol samples in the submicrometer size range were collected at a pristine tropical rainforest site and at a suburban boreal forest site as specified in Table 2. The tropical sample was collected during the Amazonian Aerosol Characterization Experiment in February 2008 (AMAZE-08, Martin et al., 2010) at the rainforest research station TT34 near Manaus, Brazil. Concurrent chemical and microscopic analyses indicate that the AMAZE sample consisted mostly of biogenic secondary organic aerosol (SOA) accounting for up to 85 % of the submicrometer particle mass (Chen et al., 2009; Gunthe et al., 2009; Martin et al., 2010; Pöschl et al., 2010).

The boreal sample was collected at the Institute of Physics of the State University of Saint-Petersburg in suburban forest environment of Petrodvoretz near the city of Saint-Petersburg, Russia, in May 2009 (SPB sample). Detailed

chemical composition data are not available for the SPB sample, but a thermal combustion method (Kuhlbusch et al., 1998) supplemented by aqueous extraction experiments (Mayol-Bracero et al., 2002) indicate that the total water-soluble fraction of the collected particulate matter was only 30 % and the water-soluble organic fraction was as low as 10 %. These values are consistent with the FDHA measurement results presented below: low hygroscopicity and relatively low importance of molecular interactions in the SPB sample.

The particles were collected by passing an air flow of $20\,L\,min^{-1}$ through a cyclone with $1\,\mu m$ cut-off diameter (URG-2000-30EHB), a silica gel diffusion drier, and a 47 mm Teflon-coated glass fiber filter (Pallflex T60A20, Pall, Germany).

Reference aerosol samples of sodium chloride (NaCl, > 99.5 %, Merck) and ammonium sulfate ((NH$_4$)$_2$SO$_4$ or AS, Fluka, > 99.5 %) were generated by nebulization of aqueous solutions with a salt mass fraction 0.1 % in deionized water (18.2 MΩ cm, Milli Q plus 185, Millipore). The sampling system and procedures were the same as applied for the atmospheric aerosol samples, except for the particle size selection using a Battelle-type pre-impactor (model I-1, PIXE International Corporation, Florida, USA) (Mitchel and Pilcher, 1959) with $1\,\mu m$ cut-off diameter at a flow rate of $1\,L\,min^{-1}$.

The size distributions of the investigated aerosols were measured with a mobility particle sizer. The mean diameters (and geometric standard deviations) of the number size distributions were: 139 nm (2.38) for AMAZE; 109.7 nm (1.77) for SPB; 81.6 nm (1.71) for AS; and 59.4 nm (1.47) for NaCl.

3.2 Water uptake measurements

Mass-based water uptake measurements were performed with a filter-based differential hygroscopicity analyzer (FDHA) using the atmospheric aerosol filter samples and reference samples collected as described above. Circular aliquots of 13 mm diameter were cut from the aerosol loaded filters and mounted in the FDHA system shown in Fig. 1. The filter loadings of the atmospheric samples are listed in Table 2, the loadings of the NaCl and AS reference samples were 0.132 mg and 0.130 mg, respectively. Details of the experimental setup and calibration are described elsewhere
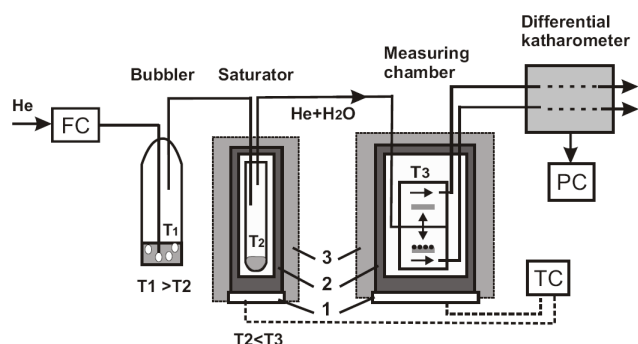
Fig. 1. Schematic set-up of the filter-based differential hygroscopicity analyzer (FDHA): FC – flow controller, TC – temperature controller, PC – computer. T1, T2, and T3 – temperature sensors. 1 – Peltier elements, 2 – copper housing (double wall cylinder), 3 – insulation.

(Mikhailov et al., 2011); the operating principles are only briefly outlined here.

In the FDHA system, the carrier gas (helium) was humidified with a bubbler (T1), equilibrated in a saturator (T2 < T1), and then passed through a pair of differential measurement cells (T3 > T2). The reference cell contains a clean filter aliquot; the other cell contains the aerosol loaded filter aliquot. The mass of water taken up by the aerosol particles on the loaded filter aliquot was determined by a differential katharometer and recorded by an analog-digital converter and a personal computer. The measurement uncertainties depend on the weighing accuracy of dry particle mass (aerosol loading), absorbed water mass (aerosol hygroscopicity), and water vapor measurement precision of the katharometer (Mikhailov et al., 2011). The experimental conditions in the measurements cells were close to ambient temperature and pressure (~ 295 K, ~ 1 atm).

In this study, the largest uncertainties in the determination of mass growth factors, G_m (Eq. 9) were associated with the AMAZE sample: $\sim 1\%$ at 30 % RH and $\sim 8\%$ at 99 % RH. The relative humidity of the FDHA water uptake measurement is determined from the temperature ratio between the water vapor saturator (T2) and the measurement cells (T3) using empirical formulas recommended by the World Meteorological Organisation (Flatau et al., 1992). The accuracy at 99 % RH was $\pm 0.06\%$ RH, resulting from accurate temperature control using a double-wall copper housing with forced thermal insulation and precise temperature measurements (± 0.01 K, 42095-Pt100; KELVIMAT 4306, Burster). The water uptake experiments were performed in two modes: hydration = increasing RH; dehydration = decreasing RH. Hydration/dehydration mass growth factor measurements took on average 10–60 min at 10–70 % RH, while above 98 % RH it took 1–2 days to reach thermodynamic equilibrium.

To avoid or minimize potential particle coagulation in the course of humidification and drying cycles we used relatively low filter loadings (~ 0.1 mg cm^{-2}). SEM analyses showed

that under these conditions the average distance between particles was larger than the expected diameter growth factors ($G_D = 2$–10 for NaCl at RH = 80–99 %) (Mikhailov et al., 2011). Moreover, the hydration and dehydration experiments were performed in multiple cycles that went up to different maximum RH values (60 %, 80 %, 99 %) and yielded consistent results, indicating that coagulation at high RH had no significant effect.

The potential particle mass lost due to evaporation was monitored by weighing the loaded filters before and after water uptake measurements. These measurements as well as subsequent hygroscopic data obtained at repetitive drying-humidifying cycles showed that the effect of particle evaporation was negligibly small for the atmospheric samples as well as the NaCl and AS reference samples.

4 Measurement results and discussion

4.1 Sodium chloride and ammonium sulfate

Figure 2a and b show the measured mass growth factors plotted against relative humidity (RH) for the sodium chloride (NaCl) and ammonium sulfate (AS) reference samples investigated in FDHA experiments. Upon hydration (increasing RH), the inorganic salt crystals exhibited stepwise deliquescence transitions at RH$_d$ values of $75.8 \pm 0.2\%$ for NaCl and $80.6 \pm 0.3\%$ for AS. The Kelvin effect correction, which is needed for polydisperse aerosol samples (cf. Appendix C), gives 75.0 % for NaCl and 79.9 % for AS. These values are in a good agreement with literature data (RH$_{d,NaCl}$ = $75.3 \pm 0.1\%$, RH$_{d,AS}$ = $79.9 \pm 0.5\%$; Tang and Munkelwitz, 1993). From the mass growth factors measured after full deliquescence, i.e., at 76 % RH for NaCl and at 81 % RH for AS, we calculated the corresponding water solubilities using the relation $C_m = 1/(G_m - 1)$ (Eq. 30). The obtained values of 0.36 ± 0.02 g g^{-1} for NaCl and 0.76 ± 0.02 g g^{-1} for AS are in a good agreement with literature data on the equilibrium solubility of these salts in water at room temperature (Stephen and Stephen, 1963; Clarke and Glew, 1985; Tang and Munkelwitz, 1994; Marcolli et al., 2004). Upon dehydration (decreasing RH), efflorescence of the solution droplets occurred at RH$_e$ values of $54 \pm 2\%$ for NaCl and $41 \pm 1\%$ for AS. The observed efflorescence thresholds are at the upper end of literature data reported for particles larger than 100 nm (35–40 % for AS, Ciobanu et al., 2010; 43–50 % for NaCl, Gao et al., 2007), which may be due to partial coagulation and impurities inducing crystallization (Martin, 2000). The dashed model lines in Figs. 2a and 2b were calculated using Eq. (30) with data of the Aerosol Inorganic Model (AIM, Clegg et al., 1998), which can be regarded as an accurate reference (Rose et al., 2008; Mikhailov et al., 2009). In these and subsequent model calculations relating water activity and relative humidity, we used Eq. (12) assuming $D_d = D_{eff}$ as explained in Appendix C (Eq. C4).
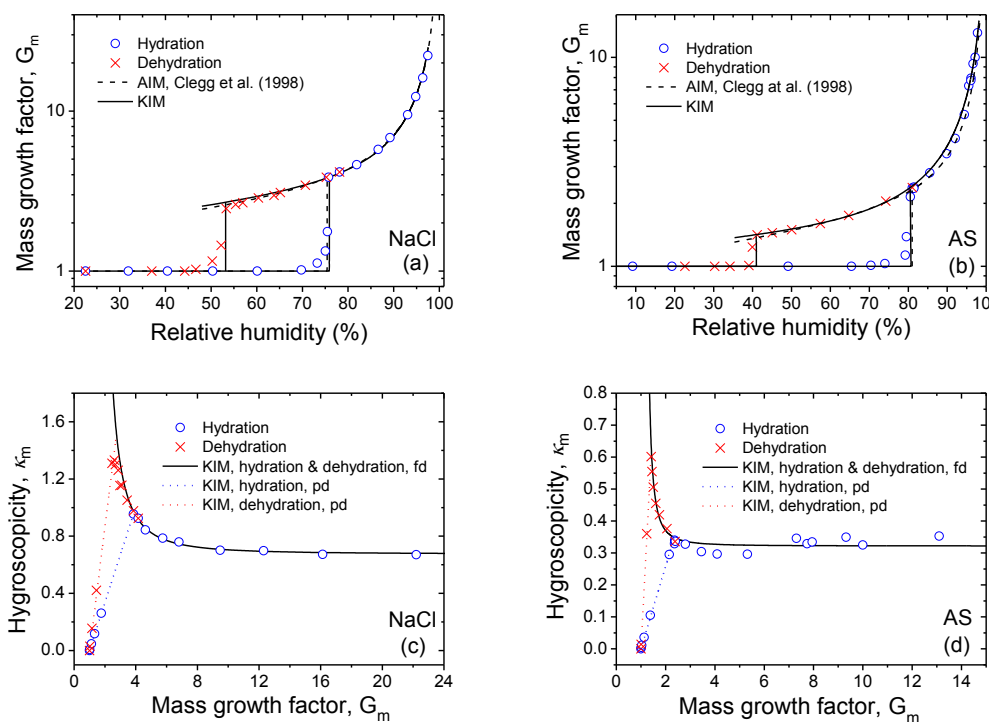
Fig. 2. Hygroscopic properties of sodium chloride (NaCl) and ammonium sulfate (AS) particles: **(a, b)** mass growth factors (G_m) observed as a function of relative humidity; **(c, d)** mass-based hygroscopicity parameters (κ_m) calculated as a function of mass growth factor (Appendix C, Eq. C2). The data points are from FDHA experiments of hydration (blue circles) and dehydration (red crosses). The lines represent different models: **(a, b)** KIM – black solid; AIM reference – black dashed; **(c, d)** KIM for fully dissolved (fd) particles (Eq.29) – black solid; KIM for partly dissolved (pd) particles (Eq. 28) – blue dotted upon hydration and red dotted upon dehydration.

Table 3. KIM fit parameters for inorganic reference salt and pure organic substance particle samples. κ_m^0 and α are the dilute hygroscopicity and self-interaction parameters obtained with KIM model Eqs. (29) and (31); n and R^2 are the number of data points and the coefficient of determination of the fit. C_m is the equilibrium water solubility determined upon deliquescence, and C_m^{ap} is the apparent solubility determined upon efflorescence.

Sample	Data*	Data source	κ_m^0	α	n	R^2	Fit equation	C_m (g g^{-1})	C_m^{ap} (g g^{-1})
NaCl	FDHA	This study	0.68 ± 0.01	2.35 ± 0.07	19	0.99	29	0.36 ± 0.02	0.58 ± 0.01
(NH$_4$)$_2$SO$_4$ (AS)	FDHA	This study	0.32 ± 0.01	0.047 ± 0.002	18	0.96	29	0.76 ± 0.02	2.44 ± 0.01
Malonic acid (MA)	Raman	Yeung and Chan (2010)	0.23 ± 0.01	$1.49 \times 10^{-3} \pm 3.5 \times 10^{-4}$	19	0.56	29	1.58 ± 0.03	13.35 ± 0.01
Levoglucosan (LG)	EDB + bulk	Peng et al. (2001)	0.22 ± 0.01	$-1.62 \times 10^{-5} \pm 1.8 \times 10^{-6}$	36	0.97	31	–	–
	EDB + bulk	Chan et al. (2005)	0.11 ± 0.01	$-5.45 \times 10^{-6} \pm 4.0 \times 10^{-7}$	36	0.98	31	–	–

* FDHA: filter-based differential hygroscopicity analyzer; EDB: electrodynamic balance, Raman: Raman micro-spectroscopy.

Figure 2c and d show the mass-based hygroscopicity parameters (κ_m) plotted against the mass growth factors measured for NaCl and AS. The κ_m values were calculated as specified in Appendix C. We used the KIM model Eq. (29) for single solute systems to fit the data points for fully deliquesced NaCl and AS (solid black lines), and the obtained best fit parameter values and standard errors of the mass-based dilute hygroscopicity parameter κ_m^0 and of the solute interaction parameter α are listed in Table 3. For NaCl, the best fit value of $\kappa_m^0 = 0.67$ corresponds to a dilute van't Hoff factor $J^0 = 2.17$ (Eq. 8) and to a volume-based dilute hygroscopicity parameter $\kappa_v^0 = 1.45$ (Eq. 7 with $\rho_d =$

2.165 g cm^{-3}). For AS, $\kappa_m^0 = 0.32$ corresponds to $J^0 = 2.35$ and to $\kappa_v^0 = 0.57$ (Eq. 7 with $\rho_d = 1.769$ g cm^{-3}), which is consistent with Petters and Kreidenweis (2007) and calculations based on a CCN experiment and the Aerosol Inorganic model (AIM) (Rose et al., 2008).

By inserting κ_m^0 and α from Table 3 in Eqs. (29) and (12), we obtained the KIM model results displayed in Fig. 2a and b (solid line). For both NaCl and AS, the KIM two parameter model is in good agreement with the measurement data as well as with the much more complex AIM multi-parameter model (dashed line).

The data points on the dry salt particle baseline in Fig. 2a and b correspond to the data points in the lower left corner of Fig. 2c and d ($G_m = 1$ and $\kappa_m = 0$). The data points in between the dry salt baseline and the hygroscopic growth curve for fully deliquesced particles indicate the co-existence of solid salt crystals with aqueous solution droplets, which can be explained by inhomogeneities in the salt particle samples (size, morphology, impurities, etc.) or non-uniform conditions in the experimental setup (spatial and temporal fluctuations in relative humidity; Biskos et al., 2006; Mikhailov et al., 2009). The KIM model Eq. (28) can be used to describe such partially deliquesced systems. With the parameters derived from the fit of Eq. (29) to the data for fully deliquesced salt samples (κ_m^0, α, and C_m as specified in Table 3), Eq. (28) yields the dotted blue model lines in Fig. 2c and d that are in good agreement with the water uptake observed during partial deliquescence upon hydration. For the data points reflecting partial efflorescence upon dehydration, we applied Eq. (28) with C_m as a free fit parameter representing the apparent solubility of the salts in the supersaturated aqueous solution droplets. The apparent solubilities corresponding to the dotted red fit lines in Fig. 2c and d are $0.58 \pm 0.01\,\mathrm{g\,g^{-1}}$ for NaCl and $2.44 \pm 0.01\,\mathrm{g\,g^{-1}}$ for AS (Table 3). These values represent the maximum salt concentration in metastable, supersaturated aqueous solution droplets at $\mathrm{RH} < \mathrm{RH_d}$.

4.2 Levoglucosan

Figure 3a shows mass growth factors of levoglucosan (LG) plotted against relative humidity. The data are from Chan et al. (2005) who used electrodynamic balance (EDB) and bulk measurement techniques and observed no stepwise deliquescence or efflorescence transitions, indicating that the samples were amorphous (Mikhailov et al., 2009). Throughout the investigated RH range of 3 % to 98 %, the observed hygroscopic growth of the amorphous organic particles is well described by a fit of the KIM model Eq. (31) for deliquesced particles, and the corresponding hygroscopicity and interaction parameters κ_m^0 and α for LG are given in Table 3. The best fit value of $\kappa_m^0 = 0.11$ corresponds to a dilute van't Hoff factor close to unity as expected for non-dissociating molecules ($J^0 = 0.99$, Eq. 8) and to a volume-based dilute hygroscopicity parameter $\kappa_v^0 = 0.18$ (Eq. 7, with $\rho_d = 1.6\,\mathrm{g\,cm^{-3}}$). The KIM two-parameter equation fits the experimental data well as the empirical three-parameter approach used in earlier studies (Mikhailov et al., 2009) and much better than the more complex UNIFAC model with group interaction parameters taken from Hansen et al. (1991), which does not capture the shape of the measured growth curve (Fig. 3a). The near-unity van't Hoff factor and the small interaction parameter reflect near-ideal solution behavior of levoglucosan in agreement with the HTDMA measurement and model results of Mikhailov et al. (2009).

4.3 Malonic acid

Figure 3b shows the hygroscopic growth of amorphous malonic acid (MA) observed by Peng et al. (2001) using electrodynamic balance (EDB) and bulk measurement techniques. The measurement data are well described by a fit of the KIM model Eq. (31), and the corresponding fit parameter values of κ_m^0 and α are given in Table 3. The best fit value of $\kappa_m^0 = 0.22$ corresponds to a dilute van't Hoff factor $J^0 = 1.33$ (Eq. 8) and to a volume-based dilute hygroscopicity parameter $\kappa_v^0 = 0.36$ (Eq. 7, with $\rho_d = 1.619\,\mathrm{g\,cm^{-3}}$). The results of the KIM two-parameter equation are nearly identical to the E-AIM results that are also displayed in Fig. 3b and are based on a more complex approach with four fit parameters (Redlich-Kister expansion; McGlashan, 1963; Clegg and Seinfeld, 2006).

Figure 4a shows the hygroscopic growth of crystalline MA observed by Yeung and Chan (2010) who used Raman micro-spectroscopy and reported water-to-solute mass ratios (WSR) that are equivalent to mass growth factors ($G_m = \mathrm{WSR} + 1$). The crystalline MA sample exhibited a stepwise deliquescence transition at 67 % RH (equilibrium solubility $C_m = 1.58\,\mathrm{g\,g^{-1}}$), and sharp changes in the position and width of the Raman signals indicated an efflorescence transition at 14 % RH. The dependence of κ_m on G_m observed for crystalline MA (Fig. 4b) is qualitatively similar to the behavior observed for crystalline NaCl and AS (Fig. 2a, b). KIM model Eq. (29) was used to fit the data points for fully deliquesced MA (Fig. 4b, solid black line), and the corresponding fit parameters are given in Table 3. The goodness of fit for the Raman data is lower than for the EDB data, but nevertheless, the fit parameters and the corresponding model lines in Fig. 4a are in good agreement with each other and with the measurement data. With the equilibrium solubility determined upon hydration, $C_m = 1.58 \pm 0.03\,\mathrm{g\,g^{-1}}$, the KIM model Eq. (28) for partially deliquesced systems yields the dotted blue model line in Fig. 4b. A fit of the same equation to the data observed upon dehydration (red dotted line) yields an apparent solubility of $C_m^{ap} = 13.35 \pm 0.01\,\mathrm{g\,g^{-1}}$.

The good agreement with measurement data for NaCl, AS, LG and malonic acid shows that the KIM model approach is well suited to describe the hygroscopic growth and stepwise deliquescence/efflorescence transitions of crystalline inorganic and organic substances as well as the gradual deliquescence/efflorescence of amorphous organic substances. The KIM model results are also in good agreement with established reference models (AIM, E-AIM), but the latter usually depend on more parameters and KIM is easier to use for efficient fitting and description of new measurement data. Eqs. (29) and (31) with the dilute hygroscopicity parameter κ_m^0 and the interaction parameter α enable efficient description of the RH and solute concentration dependence of the hygroscopicity of fully deliquesced single-component systems. Equation (28) enables the description of partially
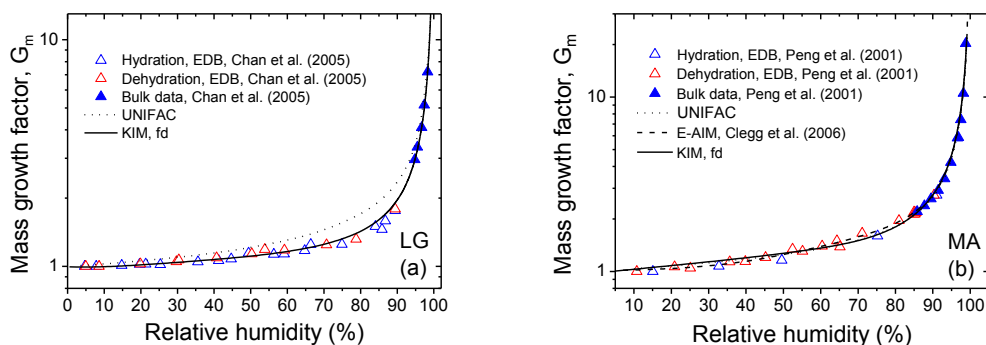
Fig. 3. Mass growth factors observed for amorphous levoglucosan (LG) and malonic acid (MA) particles as a function of relative humidity. Data points: bulk experiments (filled triangles) and EDB experiments (open triangles) of hydration (blue) and dehydration (red) from **(a)** Chan et al. (2005) and **(b)** Peng et al. (2001). Model lines: KIM for fully dissolved (fd) particles (Eq. 31) – black solid; UNIFAC – black dotted; E-AIM, Clegg et al. (2006) – black dashed.
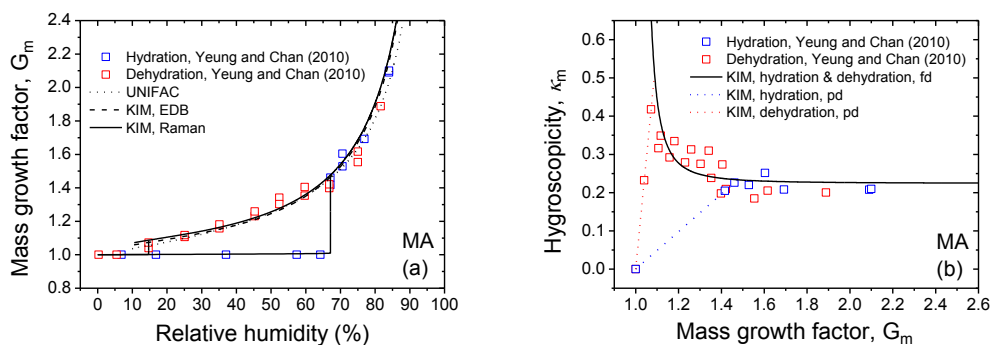

Fig. 4. Hygroscopic properties of crystalline malonic acid (MA) particles: **(a)** mass growth factors (G_m) observed as a function of relative humidity; **(b)** mass-based hygroscopicity parameters (κ_m) calculated as a function of mass growth factor (Eq. 10). Data points: micro-Raman experiments of hydration (blue) and dehydration (red) from Yeung and Chan (2010). Model lines: **(a)** UNIFAC with interaction parameters from Peng et al. (2001) – black dotted; KIM fit to micro-Raman data – black solid; KIM with fit parameters from EDB data for amorphous MA (Fig. 3b) – black dashed; **(b)** KIM for fully dissolved (fd) particles (Eq. 29) – black solid; KIM for partly dissolved (pd) particles (Eq. 28) – blue dotted upon deliquescence and red dotted upon efflorescence.

deliquesced systems, and Eq. (32) with the equilibrium solubility C_m, or the apparent solubility $C_{m,i}^{ap}$ describes the RH threshold of deliquescence and efflorescence, respectively.

4.4 Mixed malonic acid and ammonium sulfate

Figure 5 shows the hygroscopic behavior of particles consisting of mixed malonic acid and ammonium sulfate (MA-AS) with a mole ratio of 1 : 1 ($f_{MA} = 0.441$; $f_{AS} = 0.559$). The measurement data are from EDB experiments of Ling and Chan (2008) (stars), scanning EDB (SEDB) experiments of Choi and Chan (2002) (open triangles), and Raman micro-spectroscopic experiments by Yeung and Chan (2010) (open squares). Upon hydration (Fig. 5a), the mixed MA-AS particles exhibit gradual deliquescence as expected for mixed crystalline or amorphous substances (Martin, 2000; Mikhailov et al., 2009). The onset of deliquescence occurred at much lower relative humidity ($\sim 30\%$) than predicted by the E-AIM (eutonic point at $\sim 63\%$ RH, Clegg et al., 2006) and reported from earlier bulk measurements ($\sim 71\%$,

Brooks et al., 2002), indicating an amorphous state of MA as discussed below. The observed hygroscopic growth of fully deliquesced particles (RH > 75 %) is in good agreement with predictions based on the E-AIM (Clegg and Seinfeld, 2006) and on the E-ZSR model (Clegg et al., 2004).

Upon dehydration (Fig. 5b), efflorescence was observed around $\sim 20\%$ RH. In one of the particles investigated by Choi and Chan (2002), partial crystallization was observed at higher RH, but the experiment was likely influenced by contaminants (Yeung and Chan, 2010) and the data are not included in our study.

Figure 5c shows the mass-based hygroscopicity parameters plotted against the mass growth factors observed for the mixed MA-AS particles. The κ_m values were calculated by inserting the data pairs of G_m and $a_w = \text{RH}/100\%$ in Eq. (10). The observed dependence of κ_m on G_m exhibits three different sections labeled (Ia, Ib, II, and III). These sections can be classified as different regimes of hygroscopicity and described by KIM model equations as follows:
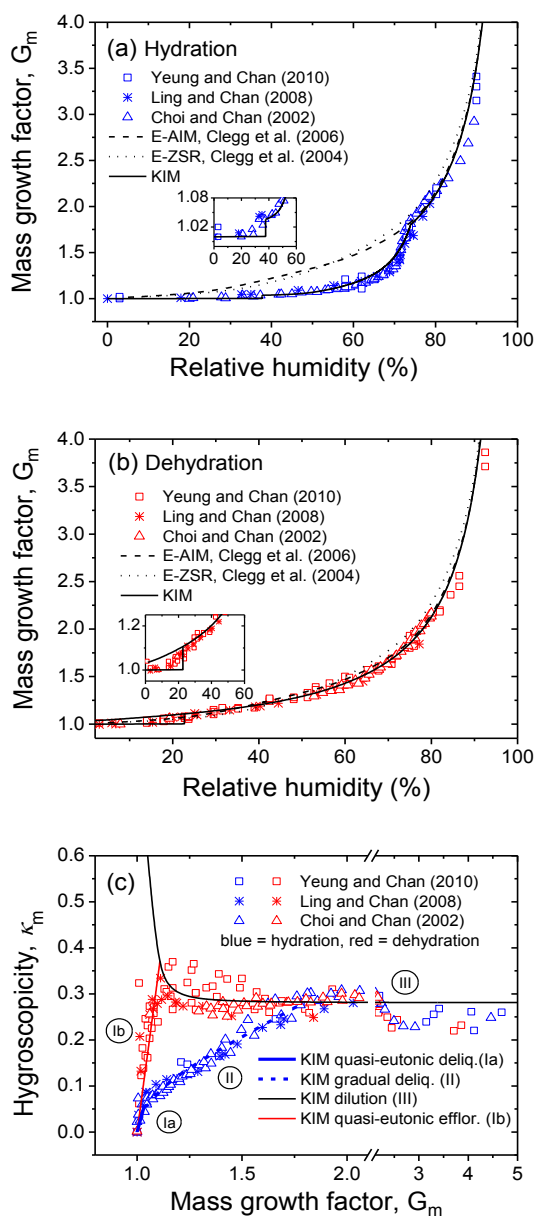
Fig. 5. Hygroscopic properties of mixed malonic acid – ammonium sulfate particles (MA-AS, mole ratio 1 : 1): **(a, b)** mass growth factors (G_m) observed as a function of relative humidity upon hydration (blue) and dehydration (red). **(c)** Mass-based hygroscopicity parameters (κ_m) calculated as a function of mass growth factor (Eq. 10). Labels Ia, Ib, II, and III indicate different regimes of hygroscopicity. Data points: EDB experiments (stars) from Ling and Chan (2008), SEDB experiments (triangles) from Choi and Chan (2002), and micro-Raman experiments (squares) from Yeung and Chan (2010). Model lines: **(a, b)** KIM – black solid; E-AIM, Clegg et al. (2006) – black dashed; E-ZSR, Clegg et al. (2004) – black dotted; **(c)** KIM: quasi-eutonic deliquescence regime – blue solid; gradual deliquescence regime – blue dashed; dilution regime – black solid; quasi-eutonic efflorescence regime – red solid.

I. The first section is a "quasi-eutonic deliquescence & efflorescence regime", where all substances are just partly dissolved and exist also in a non-dissolved state and their aqueous phase concentrations correspond to apparent solubilities as defined and discussed above (Sect. 2.3):

In the "quasi-eutonic deliquescence regime" (Ia), the linear increase of κ_m with G_m starting from $\kappa_m = 0$ at $G_m = 1$ can be described by Eq. (26):

$$\kappa_m = \left(\left(\kappa_{MA}^0 C_{m,MA}^{ap} + \kappa_{AS}^0 C_{AS}^{ap} \right) \right.$$
$$+ \left(\alpha_{MA,AS} C_{m,MA}^{ap} C_{AS}^{ap} \left(C_{m,MA}^{ap} + C_{m,AS}^{ap} \right) \right)$$
$$+ \left. \left(\alpha_{MA} \left(C_{m,MA}^{ap} \right)^3 + \alpha_{AS} \left(C_{m,AS}^{ap} \right)^3 \right) \right) (G_m - 1) \quad (33)$$

In the "quasi-eutonic efflorescence regime" (Ib), the linear decrease of κ_m with decreasing G_m towards $\kappa_m = 0$ at $G_m = 1$ can be also described by Eq. (33).

II. In the second section ("gradual deliquescence regime"), the dependence of κ_m on G_m can be described by Eq. (24), assuming that MA is fully dissolved and that AS undergoes gradual deliquescence:

$$\kappa_m = \kappa_{MA}^0 f_{MA} + \alpha_{MA,AS} \left(C_{m,AS}^{ap} \right)^2 f_{MA}$$
$$+ \left(\kappa_{AS}^0 C_{m,AS}^{ap} + \alpha_{AS} \left(C_{m,AS}^{ap} \right)^3 \right) (G_m - 1)$$
$$+ \frac{\alpha_{MA,AS} f_{MA}^2 C_{m,AS}^{ap}}{(G_m - 1)} + \frac{\alpha_{MA} f_{MA}^3}{(G_m - 1)^2}, \quad (34)$$

III. In the third section ("dilution regime"), the dependence of κ_m on G_m can be described by Eq. (27), assuming that both MA and AS are fully dissolved and undergo reversible dilution but no phase transition (reversible hygroscopic growth of fully deliquesced substances):

$$\kappa_m = \kappa_{MA}^0 f_{MA} + \kappa_{AS}^0 f_{AS}$$
$$+ \frac{\alpha_{MA,AS} f_{MA} f_{AS} + \alpha_{MA} f_{MA}^3 + \alpha_{AS} f_{AS}^3}{(G_m - 1)^2} \quad (35)$$

Using the dilute hygroscopicity and self-interaction parameters determined in single component experiments (κ_{MA}^0, κ_{AS}^0, α_{MA}, α_{AS}; Table 3), we fitted Eqs. (33)–(35) to the data points in Fig. 5c and obtained the fit parameters specified in Table 4. For the cross-interaction coefficient $\alpha_{MA,AS}$ we obtained two independent estimates from the gradual deliquescence regime (Eq. 34) and from the dilution regime (Eq. 35) that agree within statistical uncertainty (−0.032 vs. −0.031). The apparent solubility of AS in the gradual deliquescence regime obtained by a fit of Eq. (34), $C_{m,AS}^{ap} = 0.70 \, \mathrm{g \, g^{-1}}$, is close to the equilibrium solubility of pure crystalline AS

Table 4. KIM fit parameters for mixed malonic acid – ammonium sulfate particles (MA-AS, mole ratio 1 : 1). $C_{m,AS}^{ap}$ and $C_{m,MA}^{ap}$ are the apparent solubilities of ammonium sulfate and malonic acid in the specified hygroscopicity regimes, f_{AS} and f_{MA} are the mass fractions of ammonium sulfate and malonic acid in the dry particle material, and $\alpha_{MA,AS}$ is the cross-interaction parameter. n and R^2 are the number of data points and the coefficient of determination of each fit over the relevant range of mass growth factor (G_m).

Regime	G_m range	n	R^2	Fit equation	Input parameter	Best fit parameter ±standard error
Quasi-eutonic deliquescence (Ia)	1.00–1.04	13	0.58	33	$C_{m,AS}^{ap} = 0.70\,\mathrm{g\,g^{-1}}$ $\alpha_{MA,AS} = -0.032$	$C_{m,MA}^{ap} = 12.8 \pm 0.7\,\mathrm{g\,g^{-1}}$
Gradual deliquescence (II)	1.04–1.81	70	0.96	34	$f_{MA} = 0.441$	$\alpha_{MA,AS} = -0.032 \pm 0.001$ $C_{m,AS}^{ap} = 0.70 \pm 0.01\,\mathrm{g\,g^{-1}}$
Dilution (III)	1.10–4.68	93	0.19	35	$f_{AS} = 0.559$ $f_{MA} = 0.441$	$\alpha_{MA,AS} = -0.031 \pm 0.001$
Quasi-eutonic efflorescence (Ib)	1.12–1.0	15	0.84	33	$C_{m,MA}^{ap} = 12.8\,\mathrm{g\,g^{-1}}$ $\alpha_{MA,AS} = -0.032$	$C_{m,AS}^{ap} = 0.36 \pm 0.03\,\mathrm{g\,g^{-1}}$

($C_{m,AS} = 0.76\,\mathrm{g\,g^{-1}}$, Table 3). This confirms that the MA-AS particles investigated by Choi and Chan (2002), Ling and Chan (2008), and Yeung and Chan (2010) contained AS in crystalline form. The apparent solubility of MA in the quasi-eutonic deliquescence regime obtained by a fit of Eq. (34) is $C_{m,MA}^{ap} = 12.8\,\mathrm{g\,g^{-1}}$, which is close to the apparent solubility of pure MA ($C_{m,MA}^{ap} = 13.3\,\mathrm{g\,g^{-1}}$, Table 3). However, in contrast to AS, it is an order of magnitude higher than the equilibrium solubility of pure crystalline MA ($C_{m,MA} = 1.58\,\mathrm{g\,g^{-1}}$, Table 3) and the eutonic solubility of MA in crystalline MA-AS bulk samples ($C_{m,MA}^{eut} = 1.25\,\mathrm{g\,g^{-1}}$; Brooks et al., 2002), which confirms that the MA-AS particles investigated by Choi and Chan (2002), Ling and Chan (2008), and Yeung and Chan (2010) contained MA in amorphous form (apparent solubility enhancement ratio $R_{ap,MA} \approx 8$). For the quasi-eutonic efflorescence regime, a fit of Eq. (33) with $C_{m,MA}^{ap} = 12.8\,\mathrm{g\,g^{-1}}$ yields $C_{m,AS}^{ap} = 0.36\,\mathrm{g\,g^{-1}}$, which is lower than the equilibrium solubility ($0.76\,\mathrm{g\,g^{-1}}$) and apparent solubility ($2.44\,\mathrm{g\,g^{-1}}$) of pure AS. One possible explanation of the low value of $C_{m,AS}^{ap}$ obtained for the MA-AS system is partial crystallization of AS in the efflorescence-mode experiment (Braban and Abbatt, 2004; Yeung and Chan, 2010), which decreases the total concentration of the AS in solution.

By inserting the hygroscopicity, solubility and interaction parameters from Tables 3 and 4 in Eqs. (33), (34), (35) combined with Eq. (10), we obtained the KIM model results displayed in Fig. 5a and b (solid lines). For the hygroscopic growth of fully deliquesced particles (aqueous droplets), the KIM results are in agreement with both the measurement data and the more complex E-AIM and E-ZSR multi-parameter models (dashed and dotted lines). Moreover, KIM can also describe the early stages of water uptake and phase transitions in a mixture of crystalline inorganic and amorphous organic substances, which has not yet been possible with the more complex thermodynamic models as discussed

in related studies (Clegg and Seinfeld, 2006; Ling and Chan, 2008; Tong et al., 2008; Yeung et al., 2009). Upon hydration, KIM Eqs. (10) and (33) predict a stepwise onset of water absorption (quasi-eutonic deliquescence) at 37 % RH in agreement with the experimental data (insert in Fig. 5a). From the intersect of the gradual deliquescence curve (Eqs. 10 and 34) with the dilution curve (Eqs. 10 and 35) follows an RH threshold of 74 % for complete deliquescence in agreement with the measurement data and E-ZSR model results (Clegg and Seinfeld, 2006). Upon dehydration, KIM Eqs. (10) and (33) predict an efflorescence threshold of 23 % RH in agreement with the experimental data (insert in Fig. 5b).

4.5 Atmospheric aerosol samples

Figure 6a and b show the mass growth factors observed as a function of relative humidity upon hydration and dehydration of the atmospheric aerosol samples collected in the tropical rainforest of Amazonia near Manaus, Brazil (AMAZE) and in the boreal forest region near St. Petersburg, Russia (SPB) as detailed in Table 2 and Sect. 3.1. Both samples exhibit gradual and fully reversible water uptake similar to the behavior of amorphous organic substances (Mikhailov et al., 2009).

From the measurement data displayed in Fig. 6a and b we derived mass-based hygroscopicity parameters as outlined in Appendix C, using Eq. (C2). The corresponding plots of κ_m vs. G_m are shown in Fig. 6c for the AMAZE sample and in Fig. 6d for the SPB sample. In both cases, the observed dependence of κ_m on G_m exhibits three distinctly different sections or regimes of hygroscopicity. In the first section (quasi-eutonic regime, I) κ_m increases linearly with G_m, which can be described by Eq. (26) assuming quasi-eutonic conditions where multiple solutes co-exist in the partly dissolved state and their aqueous phase concentrations correspond to apparent solubilities ($C_{m,i}^{ap}$). In the second section (gradually deliquescent regime, II), κ_m exhibits a non-linear
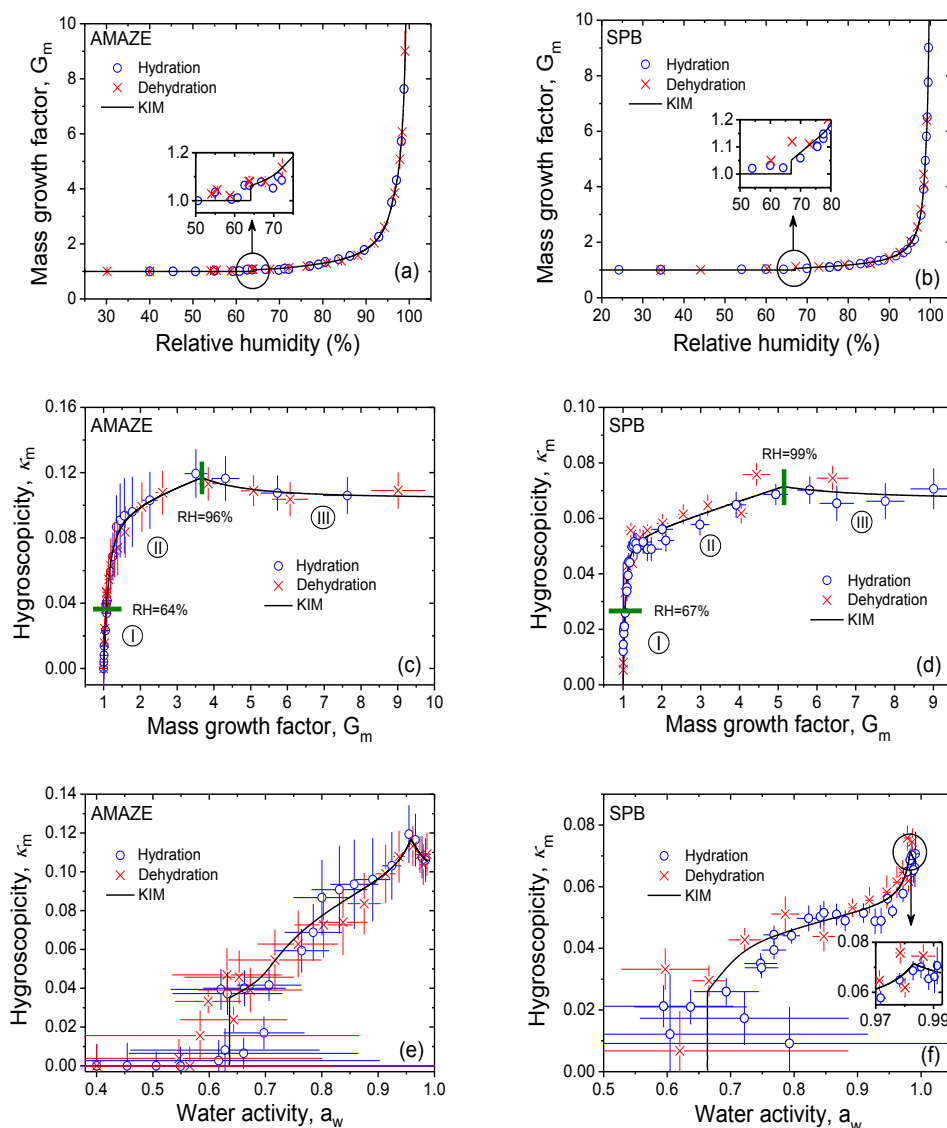
Fig. 6. Hygroscopic properties of atmospheric aerosol samples from tropical rainforest air (AMAZE) and boreal rural air (SPB, Table 2): **(a, b)** mass growth factors (G_m) observed as a function of relative humidity compared to KIM; **(c, d)** mass-based hygroscopicity parameters (κ_m) calculated as a function of mass growth factor (Appendix C, Eq. C2); and **(e, f)** mass based hygroscopicity parameters (κ_m) plotted against water activity. The data points and error bars (mean value ±standard deviation) are from FDHA experiments of hydration (blue circles) and dehydration (red crosses). The black lines are fits of KIM Eqs. (36)–(38). The labels I, II, and III indicate different regimes of hygroscopicity; the borders of the corresponding fit intervals are indicated by green bars **(c, d)**.

increase with G_m which can be described by Eq. (23) assuming gradual dissolution of multiple water soluble compounds with different solubilities ($C_{m,i}^{ap}$). In the third section (dilute regime, III), κ_m decreases with increasing G_m and becomes concentration-independent at very high values of G_m. This behavior is analogous to the behavior observed for aqueous solutions of pure substances (Fig. 2c, d; Fig. 4b) and it can be described by Eq. (27) assuming that the water-soluble fraction of the aerosol sample is fully dissolved.

The individual physico-chemical parameters involved in Eqs. (23), (26) and (27) are not readily available for at-

mospheric aerosol samples consisting of multiple chemical components with unknown molecular structures and properties. Nevertheless, Eqs. (26), (23) and (27) can be re-written as follows to fit the observed dependencies of κ_m on G_m in the different regimes of hygroscopicity:

Regime I (quasi-eutonic deliquescence/efflorescence):

$$\kappa_m = k_1 (G_m - 1) \tag{36}$$

Regime II (gradual deliquescence/efflorescence):

$$\kappa_m = k_2 + k_3 (G_m - 1) + k_4 (G_m - 1)^{-1} + k_5 (G_m - 1)^{-2} \tag{37}$$

Table 5. KIM fit parameters for the atmospheric aerosol samples collected in the Amazon (AMAZE) and in St. Petersburg (SPB). n and R^2 are the number of data points and the coefficient of determination of the fit.

Sample	Regime	G_m range	n	R^2	Fit equation	Best fit parameter ±standard error
AMAZE	Quasi–eutonic deliquescence & efflorescence (I)	1–1.06	14	0.94	36	$k_1 = 0.57 \pm 0.02$
	Gradual deliquescence & efflorescence (II)	1.06–3.6	24	0.98	37	$k_2 = 0.098 \pm 0.004$; $k_3 = 0.008 \pm 0.002$ $k_4 = -0.082 \pm 0.001$; $k_5(\mathrm{II}) = 2.7 \times 10^{-4} \pm 5 \times 10^{-5}$
	Dilution (III)	3.6–9	8	0.72	38	k_5 (III) $= 0.091 \pm 0.021$; $k_6 = 0.104 \pm 0.002$
SPB	Quasi-eutonic deliquescence & efflorescence (I)	1–1.05	11	0.65	36	$k_1 = 0.51 \pm 0.05$
	Gradual deliquescence & efflorescence (II)	1.05–5.14	11	0.82	37	$k_2 = 0.053 \pm 0.002$; $k_3 = 4.55 \times 10^{-3} \pm 7.7 \times 10^{-4}$ $k_4 = -1.47 \times 10^{-3} \pm 5.5 \times 10^{-4}$; $k_5(\mathrm{II}) = 1.0 \times 10^{-5} \pm 3 \times 10^{-5}$
	Dilution (III)	5.14–9.1	7	0.10	38	k_5 (III) $= 0.079 \pm 0.062$; $k_6 = 0.067 \pm 0.003$

Regime III (dilution):

$$\kappa_m = k_5 (G_m - 1)^{-2} + k_6 \tag{38}$$

Here k_1 to k_6 are fit parameters related to the solubility and interaction coefficients defined in Sect. 2.3:

$$k_1 = \sum_{i \in \mathrm{pd}} \kappa_{m,i}^0 C_{m,i}^{\mathrm{ap}} + \sum_{i \in \mathrm{pd}} \left(C_{m,i}^{\mathrm{ap}} \right)^2 \sum_{\substack{j \in \mathrm{pd}, \\ j > i}} \alpha_{ij} C_{m,i}^{\mathrm{ap}}$$
$$+ \sum_{i \in \mathrm{pd}} \alpha_{ii} \left(C_{m,i}^{\mathrm{ap}} \right)^3 \tag{39}$$

$$k_2 = \sum_{i \in \mathrm{pd}} \left(C_{m,i}^{\mathrm{ap}} \right)^2 \sum_{\substack{j \in \mathrm{pd}, \\ j > i}} \alpha_{ij} f_j + \sum_{i \in \mathrm{pd}} \kappa_{m,i}^0 f_i \tag{40}$$

$$k_3 = \sum_{i \in \mathrm{pd}} \kappa_{m,i}^0 C_{m,i}^{\mathrm{ap}} + \sum_{i \in \mathrm{pd}} \left(C_{m,i}^{\mathrm{ap}} \right)^2 \sum_{\substack{j \in \mathrm{pd}, \\ j > i}} \alpha_{ij} C_{m,j}^{\mathrm{ap}}$$
$$+ \sum_{i \in \mathrm{pd}} \alpha_{ii} \left(C_{m,i}^3 \right) \tag{41}$$

$$k_4 = \sum_{i \in \mathrm{fd}} f_i^2 \sum_{\substack{j \in \mathrm{pd}, \\ j > i}} \alpha_{ij} C_{m,j}^{\mathrm{ap}} \tag{42}$$

$$k_5 = \sum_{i \in \mathrm{fd}} f_i^2 \sum_{\substack{j \in \mathrm{fd}, \\ j > i}} \alpha_{ij} f_j \tag{43}$$

$$k_6 = \sum_{i \in \mathrm{fd}} \kappa_{m,i}^0 f_i \tag{44}$$

The fit parameter k_5 occurs in both Eq. (37) for regime II and Eq. (38) for regime III. Note, however, that the fit parameter values of k_5 can differ between regimes II and III, because the number of species in the aqueous phase can be different upon deliquescence ($k_5(\mathrm{II})$) and under dilute conditions ($k_5(\mathrm{III})$). According to Eq. (17), the fit parameter k_6

can be regarded as the dilute hygroscopicity parameter of the investigated sample of particulate matter (κ_m^0). The other fit parameters include interaction coefficients and solubilities.

The lines in Fig. 6c and d are fits of KIM Eqs. (36)–(38) to the experimental data, and the corresponding best fit parameters $k_1 - k_6$ are listed in Table 5. The mostly high coefficients of determination (R^2) confirm that the KIM approach can be used to describe the concentration dependence of the hygroscopicity of multi-component atmospheric aerosol samples. In spite of the very different origin of the two investigated atmospheric aerosol samples, most of the best fit parameter values were of similar magnitude.

Figure 6e and f show the hygroscopicity parameter κ_m as function of water activity. The data points were obtained by inserting the corresponding pairs of $G_m - \kappa_m$ values from Fig. 6c and d in Eq. (10). The model lines were obtained by inserting Eqs. (35)–(37) with the fit parameters from Table 5 in Eq. (10). Again the three sections I, II, and III reflect different regimes of hygroscopicity. For the quasi-eutonic regime (I), the combination of Eq. (10) and Eq. (36) yields a constant water activity value given by $a_w = (k_1 + 1)^{-1}$. This relation yields the following quasi-eutonic RH values characterizing the onset of deliquescence: 64 % for the AMAZE sample and 67 % for the SPB sample.

At and below the quasi-eutonic RH, the observed mass growth factors are close to unity (Fig. 6a and b). Thus, the ±1 % uncertainty in G_m translates into ∼ 100 % uncertainty in $G_m - 1$, which propagates further into large relative uncertainties of a_w as calculated from Eq. (10) (large horizontal error bars of the data points in the quasi-eutonic regime of Fig. 6e and f). This issue has already been discussed by Kreidenweis et al. (2008).

The gradual-deliquescence regime (II) extends up to 96 % RH for the AMAZE sample and even further up to 99 % RH for the SPB sample. Gradual deliquescence over an extended range of RH is typical for mixed multi-component particles that begin to take up water vapor at a eutonic RH value and continue to grow with increasing RH up to full dissolution of

all particle components (Wexler and Seinfeld, 1991; Martin et al., 2000; Clegg et al., 2001; Mikhailov et al., 2009).

In the dilution regime (III), the characteristic decrease of κ_m with increasing a_w is relatively steep for the AMAZE sample ($d\ln\kappa_m/d\ln a_w = 4$) and rather small for the SPB sample ($d\ln\kappa_m/d\ln a_w = 0.5$). The steep slope reflects a high value of the fit parameter $k_5(III)$, which in turn indicates strong interaction between the solute molecules in the AMAZE sample consisting mostly of SOA and small amounts of inorganic ions (~ 10–20%) (Eq. 40, Table 5) (Martin et al., 2010; Pöschl et al., 2010).

4.6 Closure between hygroscopic growth and CCN activation

In this section we test the applicability of our mass-based hygroscopicity parameter interaction model and FDHA data for closure between hygroscopic growth and CCN measurements. We used the dilute hygroscopicity parameters obtained with KIM Eq. (29) (Table 3) and Eq. (44) ($\kappa_m^0 = k_6$, Table 5) to predict the conditions of CCN activation. To calculate critical dry diameters of CCN activation ($D_{d,c}$) as a function of water vapor supersaturation (S_w) we inserted κ_m^0 in the simplified Köhler model (Eq. 15) using $\rho_w = 1.0\,\mathrm{g\,cm^{-3}}$, $\rho_d = 2.165\,\mathrm{g\,cm^{-3}}$ for NaCl, $\rho_d = 1.769\,\mathrm{g\,cm^{-3}}$ for AS. For the AMAZE sample an approximate average density of $1.3\,\mathrm{g\,cm^{-3}}$ was estimated based on Eq. (7) using the volume-based hygroscopicity $\kappa_v = 0.132$ (Gunthe et al., 2009, Table 2, CCN retrieved) and $\kappa_m^0 = k_6 = 0.104$ (Table 5). A density of $1.5\,\mathrm{g\,cm^{-3}}$ was used for the SPB sample (Virtanen et al., 2006).

Figure 7a and b show the relationship between the critical dry diameter of CCN activation and water vapor supersaturation for NaCl and AS particles predicted with KIM. For comparison the relationship is also calculated based on a full Köhler model (Köhler model AP3 of Rose et al., 2008) using the AIM for the parameterization of the water activity. The two model lines agree well with each other and show only small differences (4% at $S = 0.3\%$ for NaCl and 5% at $S = 1.2\%$ for AS). These differences are still much smaller than the differences between several experimental data obtained from direct CCN measurements (Raymond and Pandis, 2002; Giebl et al., 2002; Corrigan and Novakov, 1999; Rose et al., 2008) or derived from HTDMA measurements (Kreidenweis et al., 2005).

Figure 7c shows the relationship between the critical dry diameter of CCN activation and water vapor supersaturation for atmospheric aerosol particles predicted with KIM. For the AMAZE sample, the model predictions are in good agreement with the results of size-resolved CCN measurements (Gunthe et al., 2009) averaged over the same period as the filter sampling time (Table 2). The KIM model line falls within the error bars (standard deviations) of the experimental data points. The grey shaded area around the model line shows that uncertainties in particle density have limited
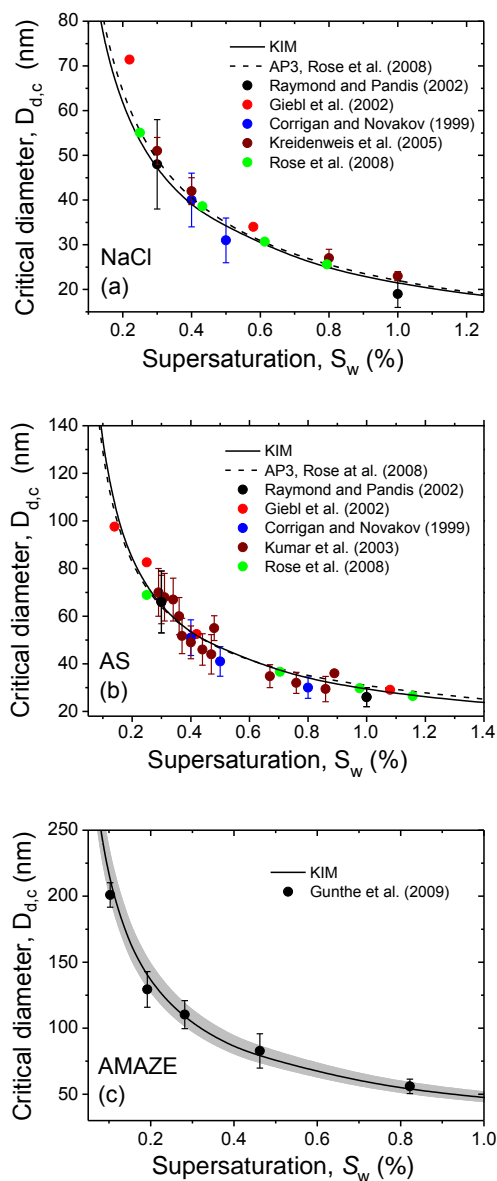

Fig. 7. Critical dry diameters of CCN activation for sodium chloride (NaCl), ammonium sulfate (AS) and atmospheric aerosol samples (AMAZE) as a function of water vapor supersaturation according to Köhler theory. Solid lines are KIM model predictions based on FDHA measurement results (κ_m^0 inserted in Eq. 15). **(a, b)** Predictions for NaCl and AS are compared against a detailed reference model (dashed lines: AIM/AP3, Rose et al., 2008) and literature data from HTDMA measurements (Kreidenweis et al., 2005) or direct CCN activation measurements (other studies). **(c)** Predictions for the Amazonian aerosol sample (AMAZE) are compared against CCN measurement data recorded while the filter sample was collected (arithmetic mean ± standard deviation). The gray shaded area denotes the uncertainty range of prediction related to particle density: center line assuming $\rho_d = 1.3\,\mathrm{g\,cm^{-3}}$, top bound with $\rho_d = 1.0\,\mathrm{g\,cm^{-3}}$ and low bound with $\rho_d = 1.6\,\mathrm{g\,cm^{-3}}$.

Table 6. CCN parameters for the reference salt samples (NaCl, (NH$_4$)$_2$SO$_4$) and for the atmospheric aerosol samples (AMAZE, SPB). κ_m^0 (= k_6) is the dilute hygroscopicity parameter (Eq. 44), ρ_d is the particle density, β is the scaling parameter and $D_{d,c}$ is the dry activation diameter calculated from Eq. (15) for water vapor supersaturations (S_w) of 0.2 % and 0.8 %.

Sample	κ_m^0	ρ_d (g cm^{-3})	β (nm^{-1})	$D_{d,c}$ (nm) $S_w = 0.2$ %	$D_{d,c}$ (nm) $S_w = 0.8$ %
NaCl	0.68	2.165	21.09	61.8	24.9
(NH$_4$)$_2$SO$_4$ (AS)	0.32	1.769	28.87	84.6	34.1
AMAZE	0.104	1.3	46.63	136.3	54.10
SPB	0.067	1.5	51.52	150.6	59.8

influence on the prediction of critical dry diameters for CCN activation: relative variations of ρ_d (1.3 ± 0.3 g cm^{-3}) lead to relative variations of ±∼ 6 % in the dry activation diameter. For the SPB sample no CCN measurement data were available, but the lower value of κ_m^0 (−35 % relative to AMAZE) implies higher activation diameter values (+10 % relative to AMAZE; Table 6).

Overall, Fig. 7 demonstrates that the mass-based hygroscopicity interaction model (KIM) is well-suited to link hygroscopic growth measurement data to CCN measurement data. The good agreement can be explained by the fact that the parameter value $\kappa_m = \kappa_m^0$ inserted in Eq. (15) represents the dilute hygroscopicity, which captures the characteristics of water uptake by dilute solution droplets as formed upon CCN activation.

5 Summary and conclusions

In this manuscript, we present a mass-based hygroscopicity parameter model approach for efficient description of concentration-dependent water uptake by pure and mixed particles including multi-component atmospheric aerosols. It can be directly used for the analysis of water uptake experiments measuring the mass of absorbed water: electrodynamic balance (EDB), particle mass analyzer (Khalizov et al., 2009), microbalance (Hatch et al., 2008), micro-Raman spectroscopy (Yeung and Chan, 2008), and filter-based techniques (Mikhailov et al., 2011; Speer et al., 2003; Lee and Hsu, 2000).

The KIM framework enables the analysis and prediction of the hygroscopic growth and phase transitions of particles with complex chemical composition. It can be applied to systems containing organic and inorganic compounds that are in amorphous and metastable states.

Equations (6)–(10) define the mass-based hygroscopicity parameter κ_m, which is equivalent to the volume-based hygroscopicity parameter introduced by Petters and Kreidenweis (2007) but independent of deviations from volume additivity. Equations (12)–(15) describe a simple Köhler model in which κ_m can be used to predict the particle critical diameter for activation to a cloud droplet.

In Eqs. (16)–(24) we develop a κ_m-interaction model (KIM) that combines a dilute hygroscopicity parameter with additional self- and cross-interaction parameters describing non-ideal solution behavior and concentration dependencies of single- and multi-component systems. For specific conditions, the main model equation (Eq. 23) can be reduced to simplified versions (Eqs. 26–27).

For particles consisting of a single organic or inorganic solute (MA, LG, NaCl, AS), Eqs. (28)–(31) provide a simple two-parameter approach (dilute hygroscopicity and self-interaction) that yields a good fit to experimental data and is in agreement with more complex multi-parameter reference models (AIM, E-AIM; Figs. 2–4). Binary mixtures of organic and inorganic solutes (MA-AS) are described by Eqs. (33)–(35) with five parameters (dilute hygroscopicities, self- and cross-interactions) providing a good fit to experimental data. Compared to established reference models (E-AIM, E-ZSR), the KIM approach agrees for fully deliquesced particles and is actually better suited for partially dissolved particles (gradual deliquescence, Fig. 5), taking into account apparent or equilibrium solubilities.

By application of KIM to FDHA measurement data of atmospheric aerosol samples, we can distinguish three different regimes of hygroscopicity: (I) a quasi-eutonic regime at low-humidity (< ∼ 70 % RH) where the solutes co-exist in aqueous and solid phases (Eq.36); (II) a gradual deliquescence regime at intermediate humidity (∼ 70 % to ∼ 96–99 % RH) where different solutes undergo gradual dissolution in the aqueous phase (Eq. 37); and (III) a dilute regime at high humidity (> ∼ 96–99 % RH) where the solutes are fully dissolved approaching their dilute hygroscopicity (Eq. 38).

In each of these regimes, the concentration dependence of κ_m can be described by simplified model equations (Eqs. 36–38) based on observable mass growth factors and a total of only six fit parameters ($k_1 - k_6$) summarizing the combined

effects of the dilute hygroscopicity parameters, self- and cross-interaction parameters, and solubilities of all involved chemical components. The parameter k_6 determined by fitting of Eq. (38) to hygroscopic growth data obtained in the dilute regime at high humidity represents the dilute hygroscopicity of the aerosol (κ_m^0) and can be used to predict CCN activation diameters as a function of water vapor supersaturation. For sodium chloride and ammonium sulfate reference particles as well as for pristine rainforest aerosols consisting mostly of secondary organic matter, we obtained good agreement between the KIM predicted critical dry diameters and directly measured dry particle activation diameters.

We are not aware of any other model that would be able and has been applied to describe the different regimes of hygroscopicity observed in our FDHA measurements and outlined above. The application of KIM and mass-based measurement techniques shall help to bridge gaps in the current understanding of water uptake by atmospheric aerosols: (1) the gap between hygroscopicity parameters determined by hygroscopic growth measurements under sub-saturated conditions and by CCN activation measurements at water vapor supersaturation, and (2) the gap between the results of simplified single parameter models widely used in atmospheric or climate science and the results of complex multi-parameter ion- and molecule-interaction models frequently used in physical chemistry and solution thermodynamics.

Appendix A

Critical supersaturation and dry diameter of CCN activation

To calculate the critical values of water vapor supersaturation and particle dry diameter, KIM (Eq. 12) can be rewritten as follows:

$$s_w = \left(\frac{\kappa_m}{G_m - 1} + 1 \right)^{-1} \exp \left(\frac{A}{D_d} \left[\frac{\rho_w}{\rho_d G_m} \right]^{1/3} \right) \text{ with}$$

$$A = \frac{4\sigma_w M_w}{RT\rho_w}. \tag{A1}$$

Taking the logarithm of Eq. (A1) and considering $\ln(x+1) \approx x$ for small x yields:

$$\ln s_w = \ln \left(\frac{\kappa_m}{G_m-1} + 1 \right)^{-1} + \frac{A}{D_d} \left[\frac{\rho_w}{\rho_d G_m} \right]^{1/3}$$

$$= -\ln \left(\frac{\kappa_m}{G_m-1} + 1 \right) + \frac{A}{D_d} \left[\frac{\rho_w}{\rho_d G_m} \right]^{1/3}$$

$$\approx -\frac{\kappa_m}{G_m - 1} + \frac{A}{D_d} \left[\frac{\rho_w}{\rho_d G_m} \right]^{1/3} \tag{A2}$$

For dilute solutions, $G_m - 1 \approx G_m$ leads to

$$\ln s_w = -\frac{\kappa_m}{G_m} + \frac{A}{D_d} \left[\frac{\rho_w}{\rho_d G_m} \right]^{1/3} \tag{A3}$$

The derivation of Eq. (A3) yields

$$\frac{d \ln s_w}{dG_m} = \frac{\kappa_m}{G_m^2} - \frac{1}{3} \frac{A}{D_d} \left(\frac{\rho_w}{\rho_d} \right)^{1/3}. \tag{A4}$$

To determine the maximum of Eq. (A3), Eq. (A4) is set to zero, and the critical value of G_m is calculated:

$$\frac{d \ln s_w}{dG_m} = \frac{\kappa_m}{G_m^2} - \frac{1}{3} \frac{A}{D_d} \left(\frac{\rho_w}{\rho_d} \right)^{1/3}$$

$$G_m^{-4/3} = 0$$

$$G_{m,c} = \left(\frac{3\kappa_m D_d}{A} \right)^{3/2} \left(\frac{\rho_d}{\rho_w} \right)^{1/2} \tag{A5}$$

To get the critical water vapor saturation ratio of CCN activation, $s_{w,c}$, we substitute Eq. (A5) into Eq. (A2):

$$\ln s_{w,c} = -\frac{\kappa_m}{\left(\frac{3\kappa_m D_d}{A} \right)^{3/2}} \left(\frac{\rho_w}{\rho_d} \right)^{1/2} + \frac{A}{D_d} \left(\frac{\rho_w}{\rho_d} \right)^{1/3}$$

$$\left[\left(\frac{3\kappa_m D_d}{A} \right)^{3/2} \left(\frac{\rho_d}{\rho_w} \right)^{1/2} \right]^{-1/3} = \left(\frac{A}{D_d} \right)^{3/2} \left(\frac{\rho_w}{\rho_d} \right)^{1/2} (3\kappa_m)^{-1/2}$$

$$-\left(\frac{A}{D_d} \right)^{3/2} \kappa_m (3\kappa_m)^{-3/2} \left(\frac{\rho_w}{\rho_d} \right)^{1/2} =$$

$$= \left(\frac{A}{D_d} \right)^{3/2} \left(\frac{\rho_w}{\rho_d} \right)^{1/2} (3\kappa_m)^{-1/2} \left[1 - \frac{\kappa_m}{3\kappa_m} \right]$$

It follows,

$$\ln s_{w,c} = \frac{2}{3} \left(\frac{A}{D_d} \right)^{3/2} \left(\frac{\rho_w}{3\kappa_m \rho_d} \right)^{1/2}$$

or

$$s_{w,c} = \exp \left[\frac{2}{3} \left(\frac{A}{D_d} \right)^{3/2} \left(\frac{\rho_w}{3\kappa_m \rho_d} \right)^{1/2} \right] \tag{A6}$$

Transforming Eq. (A6) considering that $e^x \approx x + 1$ for small x leads to

$$s_{w,c} = \exp \left[\frac{2}{3} \left(\frac{A}{D_d} \right)^{3/2} \left(\frac{\rho_w}{3\kappa_m \rho_d} \right)^{1/2} \right]$$

$$= \frac{2}{3} \left(\frac{A}{D_d} \right)^{3/2} \left(\frac{\rho_w}{3\kappa_m \rho_d} \right)^{1/2} + 1 \tag{A7}$$

Combining Eq. (A7) with $S_w (\%) = (s_w - 1) \cdot 100\%$ yields:

$$S_w (\%) = \frac{2}{3} \left(\frac{A}{D_d} \right)^{3/2} \left(\frac{\rho_w}{3\kappa_m \rho_d} \right)^{1/2} \times 100\%. \tag{A8}$$

Further transformation of Eq. (A8) yields the critical dry diameter of CCN activation, $D_{d,c}$:

$$D_{d,c} = \left[\frac{100\%}{S_w} A^{3/2} \frac{2}{3} \left(\frac{\rho_w}{3\kappa_m \rho_d} \right)^{1/2} \right]^{2/3}$$

$$= A \left(\frac{100\%}{S_w} \right)^{2/3} \left(\frac{2}{3} \right)^{2/3} \left(\frac{\rho_w}{3\kappa_m \rho_d} \right)^{1/3}$$

$$= A \left(\frac{4}{27} \frac{\rho_w}{\kappa_m \rho_d} \right)^{1/3} \left(\frac{S_w}{100\%} \right)^{-2/3}$$

or

$$D_{\text{d.c}} = \beta \times S_{\text{w}}^{-2/3} \tag{A9}$$

where $\beta = A \left(\frac{4}{27} \frac{\rho_{\text{w}}}{\kappa_{\text{m}} \rho_{\text{d}}} \right)^{1/3} \left(\frac{1}{100\,\%} \right)^{-2/3}$.

Appendix B

Relations between KIM, the osmotic coefficient and the extended ZSR model approach for multicomponent solutions

The water activity and the osmotic coefficient ϕ of a multicomponent solution are related by the expression (Clegg et al., 2001)

$$\ln a_{\text{w}} = -M_{\text{w}} \phi \sum_j \mu_j = -M_{\text{w}} \phi \frac{\sum_j n_j}{m_{\text{w}}}, \tag{B1}$$

where the summation goes over the molality μ_j or mole number n_j of all solute species (ions and molecules). From the definition of κ_{m} (Eq. 6) follows:

$$\frac{1}{m_{\text{w}}} = \left(\frac{1 - a_{\text{w}}}{a_{\text{w}}} \right) \frac{1}{\kappa_{\text{m}} m_{\text{d}}} \tag{B2}$$

Inserting the right-hand side of Eq. (B2) into Eq. (B1) and re-arranging Eq. (B2) relative to κ_{m} we obtain explicit relation between mass-based hygroscopicity parameter and regular osmotic coefficient:

$$\kappa_{\text{m}} = -\frac{M_{\text{w}}}{M_{\text{d}}} \phi \frac{(1 - a_{\text{w}})}{a_{\text{w}} \ln a_{\text{w}}}, \tag{B3}$$

where $M_{\text{d}} = m_{\text{d}} / \sum_j n_j$ is the effective molecular mass of mixed dry particle.

For dilute solution the term $(1 - a_{\text{w}})/(a_{\text{w}} \ln a_{\text{w}})$ approaches -1 and Eq. (B3) reduced to

$$\kappa_{\text{m}} \approx \kappa_{\text{m}}^0 \approx \frac{M_{\text{w}}}{M_{\text{d}}} \phi \tag{B4}$$

Equation (B4) shows that the dilute hygroscopicity, κ_{m}^0, is simply the osmotic coefficient of solution scaled by the ratio of the molar masses of water and solute.

In case of a multicomponent system the extended ZSR expression for the total mass of water at water activity, a_{w}, is given by the relation (Kirgintsev and Luk'yanov, 1966; Clegg et al., 2003):

$$m_{\text{w}} = \sum_i w_i^0 + \left(\sum_i n_i \right) \sum_i \sum_{j>i} x_i x_j \left(A_{i,j}^0 + A_{ij}^1 \lambda_{ij} + B_{ij} a_{\text{w}} \right), \tag{B5}$$

where w_i^0 mass of water in pure solution of solute i at water activity a_{w}, n_i is the number of moles of species i, $x_i = n_i / \sum_i n_i$ is the dry mole fraction of a solute i (similarly for x_j), and also $\lambda_{ij} = n_j / (n_i + n_j)$, A^0, A^1 and B are the empirical fit parameters for mixture.

Equation (B2) can be combined with Eq. (21) to obtain the respective expression for total mass of water based on the KIM :

$$m_{\text{w}} = \frac{a_{\text{w}}}{1 - a_{\text{w}}} m_{\text{d}} \left(\sum_i \kappa_{\text{m},i}^0 c_{\text{m},i} + \sum_i \sum_{j>i} \alpha_{ij} c_{\text{m},i} c_{\text{m},j} \right.$$
$$\left. + \sum_i \alpha_{ii} c_{\text{m},i}^2 \right) \tag{B6}$$

Equation (B5) and Eq. (B6) demonstrate the basic differences between KIM and ZSR models.

In the KIM one cross interaction parameters (α_{ij}) is used for every pair of solute, while in the ZSR model three empirical fit parameters are taken into account. It should also be mentioned that in the extended ZSR model the concentration effect of pure solution of the solute is not considered. The term $\sum_i w_i^0$ in Eq. (B5) assumes semi-ideal behavior where every solute may interact with the solvent but not with each other (Stokes and Robinson, 1966). The KIM contains the self-interaction coefficient (α_{ii}), which takes into account these pair interactions.

That is important for hygroscopic modeling in highly concentrated (supersaturated) solutions both for pure and for mixed particles.

From Eq. (B2), Eq. (B5) the explicit relationship between KIM and the extended ZSR model can be obtained

$$\kappa_{\text{m}} = \frac{1 - a_{\text{w}}}{a_{\text{w}}} \frac{1}{m_{\text{d}}} \tag{B7}$$

$$\left(\sum_i w_i^0 + \left(\sum_i n_i \right) \sum_i \sum_{j>i} x_i x_j \left(A_{i,j}^0 + A_{ij}^1 \lambda_{ij} + B_{ij} a_{\text{w}} \right) \right)$$

Appendix C

Kelvin correction

In this study submicron polydisperse aerosols were sampled and analyzed with the FDHA method. When calculating κ_{m} from the hygroscopic growth of polydisperse particles the Kelvin effect has to be taken into account. Therefore, the following iterative procedure was utilized to calculate κ_{m}.

The initial $\kappa_{\text{m}}^{\text{init}}$ was determined from Eq. (C1) (equivalent to Eq. 10) at a given relative humidity, s_{w}, and mass growth factor, G_{m}:

$$\kappa_{\text{m}}^{\text{init}} = \left(\frac{1}{s_{\text{w}}} - 1 \right) (G_{\text{m}} - 1) \quad \text{(under assumption that} \tag{C1}$$

$s_{\text{w}} = a_{\text{w}}$, i.e., without Kelvin effect)

Based on Eq. (12) including the Kelvin effect, κ_{m} can be written as

$$\kappa_{\text{m}} = \left(\frac{\exp \left(\frac{4\sigma_{\text{w}} M_{\text{w}}}{RT \rho_{\text{w}} D_{\text{d},i}} \left[\frac{\rho_{\text{w}}}{\rho_{\text{d}} G_{\text{m},i}} \right]^{1/3} \right)}{s_{\text{w}}} - 1 \right) (G_{\text{m},i} - 1). \tag{C2}$$

Then $G_{m,i}$ was calculated using Eq. (C2) for the dry diameter, $D_{d,i}$ of each size fraction of aerosol at given κ_m. Thus, we can obtain the wet mass, $m(D_i)$ of each aerosol fraction as follows:

$$m(D_i) = m_{d,i} G_{m,i} N(D_{d,i}), \tag{C3}$$

where $m_{d,i} = D_{d,i} \rho_d$ is the mass of dry particle, and $N(D_{d,i})$ is the concentration of the particles of a given dry size, $D_{d,i}$.

The total mass growth factor can be written as

$$G_{m,tot} = \frac{\sum_i m(D_i)}{\sum m_{d,i} N(D_{d,i})} \tag{C4}$$

The mass-based hygroscopicity parameter κ_m in Eq. (C2) is varied iteratively until the measured mass growth factor (G_m) is in coincidence with the calculated value ($G_{m,tot}$). The obtained κ_m values are shown in Fig. 2c, d and Fig. 6c, d and were used for the model fit.

To convert the modeled $G_m(a_w)$ into a $G_m(\text{RH})$ dependence we transformed Eq. (12) as follows:

$$D_{eff} = \frac{4\sigma_w M_w}{RT\rho_w} \left(\frac{\rho_w}{\rho_d G_m}\right)^{1/3} \ln\left\{s_w\left(\frac{\kappa_m}{G_m - 1}\right) + 1\right\}, \tag{C5}$$

where D_{eff} is the effective diameter of quasi-monodisperse particles with the size corrected value of κ_m (Eq. C2) at the given experimental mass growth factor G_m.

The obtained values of D_{eff} ($\pm$st. dev.) are 98.5(1.5) nm for NaCl; 171(5) nm for AS; 193(9) nm for the SPB and 233(8) nm for the AMAZE sample.

These values were used to compare experimental data with KIM calculations (Fig. 2a, b and Fig. 6a, b).

For the literature data of MA, LG and MA-AS no Kelvin correction was applied since in EDB and Raman experiments the particle diameter was varied in the range of 10–30 µm.

References

Bilde, M. and Svenningsson, B.: CCN activation of slightly soluble organics: the importance of small amounts of inorganic salt and particle phase, Tellus B, 56, 128–134, 2004.

Biskos, G., Paulsen, D., Russell, L. M., Buseck, P. R., and Martin, S. T.: Prompt deliquescence and efflorescence of aerosol nanoparticles, Atmos. Chem. Phys., 6, 4633–4642, doi:10.5194/acp-6-4633-2006, 2006.

Braban, C. F. and Abbatt, J. P. D.: A study of the phase transition behavior of internally mixed ammonium sulfate – malonic acid aerosols, Atmos. Chem. Phys., 4, 1451–1459, doi:10.5194/acp-4-1451-2004, 2004.

Brooks, S. D., Wise, M. E., Cushing, M., and Tolbert, M. A.: Deliquescence of organic/ammonium sulfate aerosol, Geophys. Res. Lett., 29, 1917, doi:10.1029/2002GL014733, 2002.

Carrico, C. M., Petters, M. D., Kreidenweis, S. M., Sullivan, A. P., McMeeking, G. R., Levin, E. J. T., Engling, G., Malm, W. C., and Collett Jr., J. L.: Water uptake and chemical composition of fresh aerosols generated in open burning of biomass, Atmos. Chem. Phys., 10, 5165–5178, doi:10.5194/acp-10-5165-2010, 2010.

Cerully, K. M., Raatikainen, T., Lance, S., Tkacik, D., Tiitta, P., Petäjä, T., Ehn, M., Kulmala, M., Worsnop, D. R., Laaksonen, A., Smith, J. N., and Nenes, A.: Aerosol hygroscopicity and CCN activation kinetics in a boreal forest environment during the 2007 EUCAARI campaign, Atmos. Chem. Phys., 11, 12369–12386, doi:10.5194/acp-11-12369-2011, 2011.

Chan, M. N., Choi, M. Y., Ng, N. L., and Chan, C. K.: Hygroscopicity of water-soluble organic compounds in atmospheric aerosols: Amino acids and biomass burning derived organic species, Environ. Sci. Technol., 39, 1555–1562, doi:10.1021/es049584l, 2005.

Chen, Q., Farmer, D. K., Schneider, J., Zorn, S. R., Heald, C. L., Karl, T. G., Guenther, A., Allan, J. D., Robinson, N., Coe, H., Kimmel, J. R., Pauliquevis, T., Borrmann, S., Pöschl, U., Andreae, M. O., Artaxo, P., Jimenez, J. L., and Martin, S. T.: Mass spectral characterization of submicron biogenic organic particles in the Amazon Basin, Geophys. Res. Lett., 36, L20806, doi:10.1029/2009GL039880, 2009.

Choi, M. Y. and Chan, C. K.: The effects of organic species on the hygroscopic behaviors of inorganic aerosols, Environ. Sci. Technol., 36, 2422–2428, doi:10.1021/es0113293, 2002.

Ciobanu, V. G., Marcolli, C., Krieger, U. K., Zuend, A., and Peter, T.: Efflorescence of ammonium sulfate and coated ammonium sulfate particles: evidence for surface nucleation, J. Phys. Chem. A, 114, 9486–9495, 2010.

Clarke, E. C. W. and Glew, D. N.: Evaluation of the thermodynamic functions for aqueous sodium chloride from equilibrium and calorimetric measurements below 154 °C, J. Phys. Chem. Ref. Data, 14, 489–609, 1985.

Clegg, S. L. and Seinfeld, J. H.: Improvement of the Zdanovskii-Stokes-Robinson model for mixtures containing solutes of different charge types, J. Phys. Chem. A, 108, 1008–1017, 2004.

Clegg, S. L. and Seinfeld, J. H.: Thermodynamic models of aqueous solutions containing inorganic electrolytes and dicarboxylic Acids at 298.15 K. 1. The acids as nondissociating components, J. Phys. Chem. A., 110, 5692–5717, 2006.

Clegg, S. L., Brimblecombe, P., and Wexler, A. S.: A thermodynamic model of the system H^+-NH_4^+-Na^+-SO_4^{2-}-NO_3^--Cl^--H_2O at 298.15 K, J. Phys. Chem. A., 102, 2155–2171, 1998.

Clegg, S. L., Seinfeld, J. H., and Brimblecombe, P.: Thermodynamic modelling of aqueous aerosols containing electrolytes and dissolved organic compounds, Aerosol Sci., 32, 713–738, doi:10.1016/S0021-8502(00)00105-1, 2001.

Clegg, S. L., Seinfeld, J. H., and Edney E. O.: Thermodynamic modelling of aqueous aerosols containing electrolytes and dissolved organic compounds. II. An extended Zdanovskii–Stokes–Robinson approach, Aerosol Sci., 34, 667–690, 2003.

Corrigan, C. E. and Novakov, T.: Cloud condensation nucleus activity of organic compounds: a laboratory study, Atmos. Environ., 33, 2661–2668, doi:10.1016/S1352-2310(98)00310-0, 1999.

Duplissy, J., DeCarlo, P. F., Dommen, J., Alfarra, M. R., Metzger, A., Barmpadimos, I., Prevot, A. S. H., Weingartner, E., Tritscher, T., Gysel, M., Aiken, A. C., Jimenez, J. L., Canagaratna, M. R., Worsnop, D. R., Collins, D. R., Tomlinson, J., and Baltensperger, U.: Relating hygroscopicity and composition of organic aerosol particulate matter, Atmos. Chem. Phys., 11, 1155–1165, doi:10.5194/acp-11-1155-2011, 2011.

Fitzgerald, J. W.: Dependence of supersaturation spectrum of CCN on aerosol size distribution and composition, J. Atmos. Sci., 30, 628–634, 1973.

Flatau, P. J., Walko, R. L., and Cotton, W. R.: Polynomial fits to saturation vapor pressure, J. Appl. Meteorology, 31, 1507–1513, 1992.

Fors, E. O., Swietlicki, E., Svenningsson, B., Kristensson, A., Frank, G. P., and Sporre, M.: Hygroscopic properties of the ambient aerosol in southern Sweden – a two year study, Atmos. Chem. Phys., 11, 8343–8361, doi:10.5194/acp-11-8343-2011, 2011.

Fredenslund, A., Jones, R. L., and Prausnitz, J. M.: Group-contribution estimation of activity coefficients in nonideal liquid mixtures, AIChE J., 21, 1086–1099, 1975.

Gao, Y., Chen, B. C., and Yu, L. T.: Efflorescence relative humidity of airborne sodium chloride particles: A theoretical investigation, Atmos. Environ., 41, 2019–2023, 2007.

Giebl, H., Berner, A., Reischl, G., Puxbaum, H., Kasper-Giebl, A., and Hitzenberger, R.: CCN activation of oxalic and malonic acid test aerosols with the University of Vienna cloud condensation nuclei counter, J. Aerosol Sci., 33, 1623–1634, doi:10.1016/S0021-8502(02)00115-5, 2002.

Good, N., Topping, D. O., Allan, J. D., Flynn, M., Fuentes, E., Irwin, M., Williams, P. I., Coe, H., and McFiggans, G.: Consistency between parameterisations of aerosol hygroscopicity and CCN activity during the RHaMBLe discovery cruise, Atmos. Chem. Phys., 10, 3189–3203, doi:10.5194/acp-10-3189-2010, 2010a.

Good, N., Topping, D. O., Duplissy, J., Gysel, M., Meyer, N. K., Metzger, A., Turner, S. F., Baltensperger, U., Ristovski, Z., Weingartner, E., Coe, H., and McFiggans, G.: Widening the gap between measurement and modelling of secondary organic aerosol properties?, Atmos. Chem. Phys., 10, 2577–2593, doi:10.5194/acp-10-2577-2010, 2010b.

Gunthe, S. S., King, S. M., Rose, D., Chen, Q., Roldin, P., Farmer, D. K., Jimenez, J. L., Artaxo, P., Andreae, M. O., Martin, S. T., and Pöschl, U.: Cloud condensation nuclei in pristine tropical rainforest air of Amazonia: size-resolved measurements and modeling of atmospheric aerosol composition and CCN activity, Atmos. Chem. Phys., 9, 7551–7575, doi:10.5194/acp-9-7551-2009, 2009.

Gunthe, S. S., Rose, D., Su, H., Garland, R. M., Achtert, P., Nowak, A., Wiedensohler, A., Kuwata, M., Takegawa, N., Kondo, Y., Hu, M., Shao, M., Zhu, T., Andreae, M. O., and Pöschl, U.: Cloud condensation nuclei (CCN) from fresh and aged air pollution in the megacity region of Beijing, Atmos. Chem. Phys., 11, 11023–11039, doi:10.5194/acp-11-11023-2011, 2011.

Gysel, M., Weingartner, E., and Baltensperger, U.: Hygroscopicity of aerosol particles at low temperatures. 2. Theoretical and experimental hygroscopic properties of laboratory generated aerosols, Environ. Sci. Technol., 36, 63–68, doi:10.1021/es010055g, 2002.

Gysel, M., Weingartner, E., Nyeki, S., Paulsen, D., Baltensperger, U., Galambos, I., and Kiss, G.: Hygroscopic properties of water-soluble matter and humic-like organics in atmospheric fine aerosol, Atmos. Chem. Phys., 4, 35–50, doi:10.5194/acp-4-35-2004, 2004.

Hancock, B. C. and Parks, M.: What is the true solubility advantage for amorphous pharmaceuticals?, Pharm. Res., 17, 397–404, 2000.

Hansen, H. K., Rasmussen, P., Fredenslund, A., Schiller, M., and Gmebling, J.: Vapor-liquid equilibria by UNIFAC group contribution. 5. Revision and extension, Ind. Eng. Chem. Res., 30, 2352–2355, 1991.

Hatch, C. D., Gierlus, K. M. Schuttlefield, J. D., and Grassian V. H.: Water adsorption and cloud condensation nuclei activity of calcite and calcite coated with model humic and fulvic acids, Atmos. Environ., 42, 5672–5684, 2008.

Huff Hartz, K. E., Rosenørn, T., Ferchak, S. R., Raymond, T. M., Bilde, M., Donahue, N. M., and Pandis, S. N.: Cloud condensation nuclei activation of monoterpene and sesquiterpene secondary organic aerosol, J. Geophys. Res., 110, D14208, doi:10.1029/2004JD005754, 2005.

Irwin, M., Good, N., Crosier, J., Choularton, T. W., and McFiggans, G.: Reconciliation of measurements of hygroscopic growth and critical supersaturation of aerosol particles in central Germany, Atmos. Chem. Phys., 10, 11737–11752, doi:10.5194/acp-10-11737-2010, 2010.

Junge, C. and McLaren, E.: Relationship of cloud nuclei spectra to aerosol size distribution and composition, J. Atmos. Sci., 28, 382–390, 1971.

Khalizov, A. F, Zhang, R., Zhang, D., Xue, H., Pagels, J., and McMurry, P. H.: Formation of highly hygroscopic soot aerosols upon internal mixing with sulfuric acid vapor, J. Geophys. Res., 114, D05208, doi:10.1029/2008JD010595, 2009.

Kirgintsev, A. and Luk'yanov, A. V.: Isopiestic investigations of ternary solutions. VIII. General treatment of the results for 34 ternary aqueous salt solutions, Russian Journal of Physical Chemistry, 40, 953–956, 1966

Krämer, L., Pöschl, U., and Niessner, R.: Microstructural rearrangement of sodium chloride condensation aerosol particles on interaction with water vapor, J. Aerosol. Sci., 31, 673–685, doi:10.1016/S0021-8502(99)00551-0, 2000.

Kreidenweis, S. M., Koehler, K., DeMott, P. J., Prenni, A. J., Carrico, C., and Ervens, B.: Water activity and activation diameters from hygroscopicity data – Part I: Theory and application to inorganic salts, Atmos. Chem. Phys., 5, 1357–1370, doi:10.5194/acp-5-1357-2005, 2005.

Kreidenweis, S. M., Petters, M. D., and DeMott, P. J.: Single-parameter estimates of aerosol water content, Environ. Res. Lett., 3, 035002, doi:10.1088/1748-9326/3/3/035002, 2008.

Kuhlbusch, T. A. J., Hertlein, A.-M., and Schütz, L. W.: Sources, determination, monitoring, and transport of carbonaceous aerosols in Mainz, Germany, Atmos. Environ., 32, 1097–1110, 1998.

Kulmala, M., Laaksonen, A., Charlson, R. J., and Korhonen, P.: Clouds without supersaturation, Nature, 388, 336–337, 1997.

Laaksonen, A., Korhonen, P., Kulmala, M., and Charlson, R. J. :Modification of the Köhler equation to include soluble trace gases and slightly soluble substances, J. Atmos. Sci., 55, 853–862, 1998.

Lee, C. T. and Hsu, W. C.: The measurement of liquid water mass associated with collected hygroscopic particles, Aerosol Sci., 31, 189–197, 2000.

Ling, T. Y. and Chan, C. K.: Partial crystallization and deliquescence of particles containing ammonium sulfate and dicarboxylic acids, J. Geophys. Res., 113, D14205, doi:10.1029/2008JD009779, 2008.

Marcolli, C. and Krieger, U. K..: Phase changes during hygroscopic cycles of mixed organic/inorganic model systems of tropospheric aerosols, J. Phys. Chem. A., 110, 1881–1893, doi:10.1021/jp0556759, 2006.

Marcolli, C., Luo, B., and Peter, T.: Mixing of the organic aerosol fractions: Liquids as the thermodynamically stable phases, J. Phys. Chem. A., 108, 2216–2224, doi:10.1021/jp036080l, 2004.

Martin, S. T.: Phase transitions of aqueous atmospheric particles, Chem. Rev., 100, 3403–3453, doi:10.1021/cr990034t, 2000.

Martin, S. T., Andreae, M. O., Althausen, D., Artaxo, P., Baars, H., Borrmann, S., Chen, Q., Farmer, D. K., Guenther, A., Gunthe, S. S., Jimenez, J. L., Karl, T., Longo, K., Manzi, A., Müller, T., Pauliquevis, T., Petters, M. D., Prenni, A. J., Pöschl, U., Rizzo, L. V., Schneider, J., Smith, J. N., Swietlicki, E., Tota, J., Wang, J., Wiedensohler, A., and Zorn, S. R.: An overview of the Amazonian Aerosol Characterization Experiment 2008 (AMAZE-08), Atmos. Chem. Phys., 10, 11415–11438, doi:10.5194/acp-10-11415-2010, 2010.

Mayol-Bracero, O. L., Guyon, P., Graham, B., Roberts, G., and Andreae, M. O.: Water-soluble organic compounds in biomass burning aerosols over Amazonia. 2. Apportionment of the chemical composition and importance of the polyacidic fraction, J. Geophys. Res., 107, 8091, doi:10.1029/2001JD000522, 2002.

McFiggans, G., Artaxo, P., Baltensperger, U., Coe, H., Facchini, M. C., Feingold, G., Fuzzi, S., Gysel, M., Laaksonen, A., Lohmann, U., Mentel, T. F., Murphy, D. M., O'Dowd, C. D., Snider, J. R., and Weingartner, E.: The effect of physical and chemical aerosol properties on warm cloud droplet activation, Atmos. Chem. Phys., 6, 2593–2649, doi:10.5194/acp-6-2593-2006, 2006.

McGlashan, M. L.: Deviations from Raoult's law, J. Chem. Educ., 40, 516–518, 1963.

Metzger, S., Steil, B., Xu, L., Penner, J. E., and Lelieveld, J.: New representation of water activity based on a single solute specific constant to parameterize the hygroscopic growth of aerosols in atmospheric models, Atmos. Chem. Phys., 12, 5429–5446, doi:10.5194/acp-12-5429-2012, 2012.

Mikhailov, E., Vlasenko, S., Niessner, R., and Pöschl, U.: Interaction of aerosol particles composed of protein and saltswith water vapor: hygroscopic growth and microstructural rearrangement, Atmos. Chem. Phys., 4, 323–350, doi:10.5194/acp-4-323-2004, 2004.

Mikhailov, E., Vlasenko, S., Martin, S. T., Koop, T., and Pöschl, U.: Amorphous and crystalline aerosol particles interacting with water vapor: conceptual framework and experimental evidence for restructuring, phase transitions and kinetic limitations, Atmos. Chem. Phys., 9, 9491–9522, doi:10.5194/acp-9-9491-2009, 2009.

Mikhailov, E. F., Merkulov, V. V., Vlasenko, S. S., and Pöschl, U.: Filter-based differential hygroscopicity analyzer, Izvestya Atmospheric and Oceanic Physics, 47, 747–759, 2011.

Mitchell, R. I. and Pilcher, J. M.: Improved cascade impactor for measuring aerosol particle sizes, Industrial and Engineering Chemistry, 51, 1039–1042, 1959.

Mochida, M., Kuwata, M., Miyakawa, T., Takegawa, N., Kawamura, K., and Kondo, Y.: Relationship between hygroscopicity and cloud condensation nuclei activity for urban aerosols in Tokyo, J. Geophys. Res., 111, D23204, doi:10.1029/2005JD006980, 2006.

Mosharraf, M. and Nyström, C.: The effect of dry mixing on the apparent solubility of hydrophobic, sparingly soluble drugs, Europ. J. Pharm. Sci., 9, 145–156, 1999.

Murdande, S. B., Pikal, M. J., Shanker, R. M., and Bogner, R. H.: Solubility advantage of amorphous pharmaceuticals, II. Application of quantitative thermodynamic relationships for prediction of solubility enhancement in structurally diverse insoluble pharmaceuticals, Pharm. Res., 27, 2704–2714, 2010.

Murdande, S. B., Pikal, M. J., Shanker, R. M., and Bogner, R. H.: Aqueous solubility of crystalline and amorphous drugs: challenges in measurement, Pharm. Develop. Technol., 16, 187–200, 2011.

Peng, C., Chan M. N., and Chan, C. K.: The hygroscopic properties of dicarboxylic and multifunctional acids: Measurements and UNIFAC predictions, Environ. Sci. Technol., 35, 4495–4501, 2001.

Petters, M. D. and Kreidenweis, S. M.: A single parameter representation of hygroscopic growth and cloud condensation nucleus activity, Atmos. Chem. Phys., 7, 1961–1971, doi:10.5194/acp-7-1961-2007, 2007.

Petters, M. D. and Kreidenweis, S. M.: A single parameter representation of hygroscopic growth and cloud condensation nucleus activity – Part 2: Including solubility, Atmos. Chem. Phys., 8, 6273–6279, doi:10.5194/acp-8-6273-2008, 2008.

Petters, M. D., Carrico, C. M., Kreidenweis, S. M., Prenni, A. J., DeMott, P. J., Collett, J. L., and Moosmüller, H.: Cloud condensation nucleation activity of biomass burning aerosol, J. Geophys. Res., 114, D22205, doi:10.1029/2009JD012353, 2009.

Pöschl, U., Martin, S. T., Sinha, B., Chen, Q., Gunthe, S. S., Huffman, J. A., Borrmann, S., Farmer, D. K., Garland, R. M., Helas, G., Jimenez, J.L., King, S. M., Manzi, A., Mikhailov, E., Pauliquevis, T., Petters, M. D., Prenni, A. J., Roldin, P., Rose, D., Schneider, J., Su, H., Zorn, S. R., Artaxo, P., and Andreae, M. O.: Rainforest Aerosols as Biogenic Nuclei of Clouds and Precipitation in the Amazon, Science, 329, 1513–1516, doi:10.1126/science.1191056, 2010.

Pringle, K. J., Tost, H., Pozzer, A., Pöschl, U., and Lelieveld, J.: Global distribution of the effective aerosol hygroscopicity parameter for CCN activation, Atmos. Chem. Phys., 10, 5241–5255, doi:10.5194/acp-10-5241-2010, 2010.

Pruppacher, H. R. and Klett, J. D.: Microphysics of clouds and precipitation, Kluwer Academic Publishers, Dordrecht, 2000.

Raymond T. M. and Pandis S. N.: Cloud activation of single-component organic aerosol particles, J. Geophys. Res., 107,

4787, doi:10.1029/2002JD002159, 2002.

Raymond, T. M. and Pandis, S. N.: Formation of cloud droplets by multicomponent organic particles, J. Geophys. Res., 108, 4469, doi:10.1029/2003JD003503, 2003.

Rissler, J., Swietlicki, E., Zhou, J., Roberts, G., Andreae, M. O., Gatti, L. V., and Artaxo, P.: Physical properties of the sub-micrometer aerosol over the Amazon rain forest during the wet-to-dry season transition – comparison of modeled and measured CCN concentrations, Atmos. Chem. Phys., 4, 2119–2143, doi:10.5194/acp-4-2119-2004, 2004.

Roberts, G. C., Day, D. A., Russell, L. M., Dunlea, E. J., Jimenez, J. L., Tomlinson, J. M., Collins, D. R., Shinozuka, Y., and Clarke, A. D.: Characterization of particle cloud droplet activity and composition in the free troposphere and the boundary layer during INTEX-B, Atmos. Chem. Phys., 10, 6627–6644, doi:10.5194/acp-10-6627-2010, 2010.

Rose, D., Gunthe, S. S., Mikhailov, E., Frank, G. P., Dusek, U., Andreae, M. O., and Pöschl, U.: Calibration and measurement uncertainties of a continuous-flow cloud condensation nuclei counter (DMT-CCNC): CCN activation of ammonium sulfate and sodium chloride aerosol particles in theory and experiment, Atmos. Chem. Phys., 8, 1153–1179, doi:10.5194/acp-8-1153-2008, 2008.

Rose, D., Nowak, A., Achtert, P., Wiedensohler, A., Hu, M., Shao, M., Zhang, Y., Andreae, M. O., and Pöschl, U.: Cloud condensation nuclei in polluted air and biomass burning smoke near the mega-city Guangzhou, China – Part 1: Size-resolved measurements and implications for the modeling of aerosol particle hygroscopicity and CCN activity, Atmos. Chem. Phys., 10, 3365–3383, doi:10.5194/acp-10-3365-2010, 2010.

Rose, D., Gunthe, S. S., Su, H., Garland, R. M., Yang, H., Berghof, M., Cheng, Y. F., Wehner, B., Achtert, P., Nowak, A., Wiedensohler, A., Takegawa, N., Kondo, Y., Hu, M., Zhang, Y., Andreae, M. O., and Pöschl, U.: Cloud condensation nuclei in polluted air and biomass burning smoke near the mega-city Guangzhou, China – Part 2: Size-resolved aerosol chemical composition, diurnal cycles, and externally mixed weakly CCN-active soot particles, Atmos. Chem. Phys., 11, 2817–2836, doi:10.5194/acp-11-2817-2011, 2011.

Seinfeld, J. H. and Pandis, S. N.: Atmospheric Chemistry and Physics: From Air Pollution to Climate Change, John Wiley and Sons, Inc., New York, 2006.

Setschenov, J.: Über die Konstitution der Salzlösungen aufgrund ihres Verhaltens zu Kohlensäure, Z. Phys. Chem., 4, 117–125, 1889.

Shulman, M. L., Jacobson, M. C., Carlson, R. J., Synovec, R. E., and Young, T. E.: Dissolution behavior and surface tension effects of organic compounds in nucleating cloud droplets, Geophys. Res. Lett., 23, 277–280, doi:10.1029/95GL03810, 1996.

Sjogren, S., Gysel, M., Weingartner, E., Baltensperger, U., Cubison, M. J., Coe, H., Zardini, A. A., Marcolli, C., Krieger, U. R., and Peter, T.: Hygroscopic growth and water uptake kinetics of two-phase aerosol particles consisting of ammonium sulphate, adipic and humic acid mixtures, J. Aerosol Sci., 38, 157–171, 2007.

Speer, R. E., Edney, E. O., and Kleindenst, T. E.: Impact of organic compounds on the concentrations of liquid water in ambient PM2:5, Aerosol Sci., 34, 63–77, 2003.

Stephen, H. and Stephen, T. (Eds.): Solubilities of inorganic and organic compounds, Pergamon Press, Oxford, 1963.

Stokes, R. H. and Robinson, R. A.: Interactions in aqueous nonelectrolyte solutions: I. Solute-solvent equilibria, J. Phys. Chem., 70, 2126–2130, 1966.

Sullivan, R. C., Moore, M. J. K., Petters, M. D., Kreidenweis, S. M., Roberts, G. C., and Prather, K. A.: Effect of chemical mixing state on the hygroscopicity and cloud nucleation properties of calcium mineral dust particles, Atmos. Chem. Phys., 9, 3303–3316, doi:10.5194/acp-9-3303-2009, 2009.

Svenningsson, B., Rissler, J., Swietlicki, E., Mircea, M., Bilde, M., Facchini, M. C., Decesari, S., Fuzzi, S., Zhou, J., Mønster, J., and Rosenørn, T.: Hygroscopic growth and critical supersaturations for mixed aerosol particles of inorganic and organic compounds of atmospheric relevance, Atmos. Chem. Phys., 6, 1937–1952, doi:10.5194/acp-6-1937-2006, 2006.

Tang, I. N. and Munkelwitz, H. R.: Composition and temperature dependence of the deliquescence properties of hygroscopic aerosol, Atmos. Environ., 27A, 467–473, doi:10.1016/0960-1686(93)90204-C, 1993.

Tang, I. N. and Munkelwitz, H. R.: Water activities, densities, and refractive indices of aqueous sulfates and sodium nitrate droplets of atmospheric importance, J. Geophys. Res., 20, 18801–18808, 1994.

Tong, C., Clegg, L. C., and Seinfeld, J. H.: Comparison of activity coefficient models for atmospheric aerosols containing mixtures of electrolytes, organics, and water, Atmos. Environ., 42, 5459–5482, 2008.

Topping, D. O., McFiggans, G. B., and Coe, H.: A curved multi-component aerosol hygroscopicity model framework: Part 1 – Inorganic compounds, Atmos. Chem. Phys., 5, 1205–1222, doi:10.5194/acp-5-1205-2005, 2005a.

Topping, D. O., McFiggans, G. B., and Coe, H.: A curved multi-component aerosol hygroscopicity model framework: Part 2 – Including organic compounds, Atmos. Chem. Phys., 5, 1223–1242, doi:10.5194/acp-5-1223-2005, 2005b.

Virtanen, A., Rönkkö, T., Kannosto, J., Ristimäki, J., Mäkelä, J. M., Keskinen, J., Pakkanen, T., Hillamo, R., Pirjola, L., and Hämeri, K.: Winter and summer time size distributions and densities of traffic-related aerosol particles at a busy highway in Helsinki, Atmos. Chem. Phys., 6, 2411–2421, doi:10.5194/acp-6-2411-2006, 2006.

Wang, Z., King, S. M., Freney, E., Rosenoern, T., Smith, M. L., Chen, Q., Kuwata, M., Lewis, E. R., Pöschl, U., Wang, W., Buseck, P. R., and Martin, S. T.: The Dynamic Shape Factor of Sodium Chloride Nanoparticles as Regulated by Drying Rate, Aerosol Sci. Technol., 44, 939–953, doi:10.1080/02786826.2010.503204, 2010.

Wex, H., Stratmann, F., Hennig, T., Hartmann, S., Niedermeier, D., Nilsson, E., Ocskay, R., Rose, D., Salma, I., and Ziese, M.: Connecting hygroscopic growth at high humidities to cloud activation for different particle types, Environ. Res. Lett., 3, 1–10, doi:10.1088/1748-9326/3/3/035004, 2008.

Wexler, A. S. and Clegg, S. L.: Atmospheric aerosol models for systems including the ions H^+, NH_4+, Na^+, SO_4^{2-}, NO_3^-, Cl^-, Br^-, and H_2O, J. Geophys. Res., 107, ACH 14-1–ACH 14-14, doi:10.1029/2001JD000451, 2002.

Wexler, A. S. and Seinfeld, J. H.: Second-generation inorganic aerosol model, Atmos. Environ., 25A, 2731–2748, doi:10.1016/0960-1686(91)90203-J, 1991.

Yeung, M. C. and Chan, C. K.: Water content and phase transitions in particles of inorganic and organic species and their mixtures using micro-Raman spectroscopy, Aerosol Sci. Technol., 44, 269–280, 2010.

Yeung, M. C., Lee, A. K. Y., and Chan, C. K.: Phase transition and hygroscopic properties of internally mixed ammonium sulfate and adipic acid (AS-AA) particles by optical microscopic imaging and Raman spectroscopy, Aerosol Sci. Technol., 43, 387–399, 2009.

Zardini, A. A., Sjogren, S., Marcolli, C., Krieger, U. K., Gysel, M., Weingartner, E., Baltensperger, U., and Peter, T.: A combined particle trap/HTDMA hygroscopicity study of mixed inorganic/organic aerosol particles, Atmos. Chem. Phys., 8, 5589–5601, doi:10.5194/acp-8-5589-2008, 2008.

Zuend, A., Marcolli, C., Luo, B. P., and Peter, T.: A thermodynamic model of mixed organic-inorganic aerosols to predict activity coefficients, Atmos. Chem. Phys., 8, 4559–4593, doi:10.5194/acp-8-4559-2008, 2008.

Zuend, A., Marcolli, C., Booth, A. M., Lienhard, D. M., Soonsin, V., Krieger, U. K., Topping, D. O., McFiggans, G., Peter, T., and Seinfeld, J. H.: New and extended parameterization of the thermodynamic model AIOMFAC: calculation of activity coefficients for organic-inorganic mixtures containing carboxyl, hydroxyl, carbonyl, ether, ester, alkenyl, alkyl, and aromatic functional groups, Atmos. Chem. Phys., 11, 9155–9206, doi:10.5194/acp-11-9155-2011, 2011.